C FILE COPY

(4)

20030128178

AD_____

REPORT #1

SPATIAL RELATIONS BETWEEN DRUG BINDING SITES ON THE SURFACE OF THE ACETYLCHOLINE RECEPTOR: PREPARATION AND INTERACTION OF FLUORESCENT -TOXINS AND DECIDIUM WITH THE ACETYLCHOLINE RECEPTOR

ANNUAL REPORT

AD-A188 581

DAVID A. JOHNSON, PH.D.

DTIC
ELECTE
DEC 17 1987
S D
D

OCTOBER 15, 1985

SUPPORTED BY

U.S. ARMY RESEARCH AND DEVELOPMENT COMMAND
FORT DETRICK, FREDERICK, MARYLAND 21701-5012

UNIVERSITY OF CALIFORNIA, RIVERSIDE
RIVERSIDE, CALIFORNIA 92521-0121

APPROVED FOR RELEASE; DISTRIBUTION UNLIMITED

87 12 11 079

SPATIAL RELATIONSHIPS BETWEEN DRUG BINDING SITES ON THE SURFACE OF THE ACETYLCHOLINE RECEPTOR: PREPARATION AND INTERACTION OF FLUORESCENT α-TOXINS AND DECIDIUM WITH THE ACETYLCHOLINE RECEPTOR

Annual Report

David A. Johnson, Ph.D.

October 15, 1985

Supported by

U.S. ARMY MEDICAL RESEARCH AND DEVELOPMENT COMMAND
Fort Detrick, Frederick, Maryland 21701-5012

Contract No. DAMD17-84-C-4187

University of California, Riverside
Riverside, California 92521-0121

Approved for public release; distribution unlimited

The findings in this report are not to be construed as an official Department of the Army position unless so designated by other authorized documents.

SECURITY CLASSIFICATION OF THIS PAGE (When Data Entered)

REPORT DOCUMENTATION PAGE		READ INSTRUCTIONS BEFORE COMPLETING FORM
1. REPORT NUMBER	2. GOVT ACCESSION NO.	3. RECIPIENT'S CATALOG NUMBER
4. TITLE (and Subtitle) SPATIAL RELATIONS BETWEEN DRUG BINDING SITES ON THE SURFACE OF THE ACETYLCHOLINE RECEPTOR		5. TYPE OF REPORT & PERIOD COVERED Annual—September 15, 1984-September 14, 1985 6. PERFORMING ORG. REPORT NUMBER
7. AUTHOR(s) David A. Johnson		8. CONTRACT OR GRANT NUMBER(s) DAMD-17-84-4187
9. PERFORMING ORGANIZATION NAME AND ADDRESS University of California, Riverside Riverside, California 92521		10. PROGRAM ELEMENT, PROJECT, TASK AREA & WORK UNIT NUMBERS 62734A 3M162734A875.AI.457
11. CONTROLLING OFFICE NAME AND ADDRESS U.S. Army Medical Reseach & Development Command Fort Detrick Frederick, Maryland 21701-5012		12. REPORT DATE October 15, 1985 13. NUMBER OF PAGES 62
14. MONITORING AGENCY NAME & ADDRESS(if different from Controlling Office)		15. SECURITY CLASS. (of this report) Unclassified 15a. DECLASSIFICATION/DOWNGRADING SCHEDULE

16. DISTRIBUTION STATEMENT (of this Report)

Approved for public release; distribution

17. DISTRIBUTION STATEMENT (of the abstract entered in Block 20, if different from Report)

18. SUPPLEMENTARY NOTES

19. KEY WORDS (Continue on reverse side if necessary and identify by block number)

acetylcholine, acetylcholine receptor, -toxin, Torpedo californica, fluorescein isothiocyanate, isoelectric focusing, phencyclidine, BC3H-1 cells, decidium, carbachol, fluorescence probes.

20. ABSTRACT (Continue on reverse side if necessary and identify by block number)

This report describes the development of fluorescent probes of the nicotinic acetylcholine receptor and their use in an analysis of drug and cobra α-toxin interaction with the acetylcholine receptor. Section I develops a new theoretical framework in which to use fluorescence quenching techniques to analyze the solute accessiblity to fluorophores on the surface of macromolecules. This framework is utilized in an analysis of the interaction of α-toxin labeled with fluorescein isothiocyanate (FITC) at N^{ϵ} postion of

DD FORM 1 JAN 73 1473 EDITION OF 1 NOV 65 IS OBSOLETE

SECURITY CLASSIFICATION OF THIS PAGE (When Data Entered)

lysine-23 ([FITC-N^{ϵ}-lysine-23]-α-toxin) with the acetylcholine receptor. We show that when α-toxin binds to the receptor, the region around the lysine-23 and α-toxin is completely accessible to soluble. As more site-specifically labeled toxins are prepared, it will be possible to obtain a clearer picture of the disposition of the α-toxin molecule on the surface of the receptor. Section II summarizes the characterization of the interaction of a novel decamethonium homolog, decidium, with the acetylcholine receptor. Measurement of the inhibition of the initial rate of [^{125}I]-α-toxin binding to *Torpedo californica* electroplax membranes and BC3H-1 cells, inhibition of carbachol-stimulated ^{22}Na influx into BC3H-1 cells, inhibition of [^{3}H]-phencyclidine binding to *Torpedo* membranes, and fluorescence spectroscopy are utilized in these analyses. Decidium is shown to bind to both the agonist/antagonist and noncompetitive blocking binding sites on the surface of the receptor and to display specific spectral shifts associated with the interaction with each class of drug binding site. Fluorescence energy transfer studies between decidium and [FITC-N^{ϵ}-lysine-23]-α-toxin indicate some proximity between the α-toxin binding sites and the lipid bilayer. Section III summarizes our progress in site-specifically labeling α-toxin with FITC, erythrosin isothiocyanate (EITC), and tetramethylrhodamine isothiocyanate (TRITC). Utilizing new high resolution isoelectric focusing techniques, it should be possible to isolate semipreparative quantities of site-specifically labeled α-toxins.

Accesion For
NTIS CRA&I ☑
DTIC TAB ☐
Unannounced ☐
Justification
By
Distribution/
Availability Codes
Dist | Avail and/or Special
A-1

SUMMARY

This report described the development of fluorescent probes of the nicotinic acetylcholine receptor and their use in an analysis of drug and α-toxin interaction with the acetylcholine receptor. Section I develops a new theoretical framework with which to use fluorophores on the surface of macromolecules. This framework is utilized in an analysis of the interaction of fluorescein isothiocyanates (FITC)-N^{ϵ}-lysine-23-α-toxin with the acetylcholine receptor. We show that when α-toxin binds to the receptor, the region around the α-toxin's lysine 23 is completely accessible to the solute. As more site-specifically labeled toxins are prepared, it will be possible to obtain a clearer picture of the disposition of the α-toxin molecule on the surface of the receptor. Section II summarizes the characterization of the interaction of a novel decamethonium homolog, decidium, with the acetylcholine receptor. Decidium is shown to bind to both the agonist/antagonist and noncompetitive blocking binding sites on the surface of the receptor and displays specific spectral shifts associated with the interaction with each class of drug binding site. Fluorescence energy transfer studies between decidium and FITC-N^{ϵ}-lysine-23-α-toxin indicate some proximity of the α-toxin binding sites and the lipid bilayer. Section III summarizes our progress in site-specifically labeling α-toxin with FITC, erythrosin isothiocyanate (EITC), and tetramethylrhodamine isothiocyanate (TRITC). Utilizing new high resolution isoelectric focusing techniques, it should be possible to isolate semipreparative quantities of site-specifically-labeled α-toxins.

FOREWORD

In conducting the research described in this report, the investigators adhered to the "Guide for the Care and Use of the Laboratory Animals," prepared by the Committee on Care and Use of Laboratory Animals of the Institute of Laboratory Animal Resources, National Research Council (DHEW Publication No. (NIH) 78-23, Revised 1978).

Citation of commercial organizations and trade names in this report do not constitute an official Department of the Army endorsement or approval of the products or services of these organizations.

TABLE OF CONTENTS

	Page
Title Page	1
Summary	4
Foreword	5
Table of Contents	6
List of Figures	7
List of Tables	9
Background	10
Section I: Solute accessibility to fluorescein isothiocyanate-N^{ϵ}-lysine-23-cobra-α-toxin bound to the acetylcholine receptor	14
Section II: Interaction of decidium with the acetylcholine receptor	25
Section III: Progress report on efforts to site-specifically label α-toxin with FITC, EITC, and TRITC	43
Bibliography	55
List of Abbreviations	61
Distribution List	62

LIST OF FIGURES

		Page
Fig. 1	Model of Acetylcholine Receptor	11
Fig. 2	Sole and Stockmaker Model	17
Fig. 3	Theoretical Plots of k_{MQ}/k_{FQ} vs molecular weight and F_{MQ}	21
Fig. 4	Nanosecond fluorescent decay curves of FITC-toxin	22
Fig. 5	Stern-Volmer plots of KI quenching of FITC-toxin	23
Fig. 6	Structure of decidium	26
Fig. 7	Decidium inhibition of α-toxin binding	36
Fig. 8	Decidium inhibition of agonist activation	37
Fig. 9	Decidium and meproadifen effect on agonist binding	38
Fig. 10	Decidium inhibition of ACh and PCP binding	39
Fig. 11	Excitation spectra of decidium bound to AChR	40
Fig. 12	Emission spectra of decidium bound to AChR	41
Fig. 13	Spectral relation between FITC-toxin and decidium	42
Fig. 14	CM-52 elution profile of FITC-toxin	45
Fig. 15	Reaction scheme for citraconic anhydride modification	46
Fig. 16	Serva polyacrylamide isoelectric focusing of citraconic-anhydride-modified α-toxin	47
Fig. 17	Serva polyacrylamide isoelectric focusing of FITC and citraconic-anhydride-modified α-toxin	48
Fig. 18	Column IEF of unmodified and modified FITC-toxin on an LKB column	49
Fig. 19	Appearance of isoelectric focused FITC-toxin reaction mixture on IEF column	50
Fig. 20	BIO REX-70 elution profile of EITC-labeled toxin	51
Fig. 21	Serva polyacrylamide isoelectric focusing of EITC-toxin reaction mixture	52

Fig. 22 Appearance of TRITC-toxin reaction mixture on LKB column 53

Fig. 23 Isoelectric focusing elution profile of TRITC-labeled toxin 54

LIST OF TABLES

		Page
Table I.	Summary of the Stern-Volmer quenching constants the fluorescence decay rates, and the bimolecular quenching rate constant of fluorescein, FITC-toxin free in solution and bound to the acetylcholine receptor calculated utilizing Eq. 2.	24
Table II.	Nanosecond fluorescence decay of FITC-lysine-23-α-toxin bound to 15% of the α-toxin binding sites on the surface of the AChR (membrane-associated and solubilized) in the presence of decidium (20 μM) and PCP (10 mM). The fluorescence lifetime of FITC-Toxin bound to the AChR is 3.8-3.9 ns.	33

BACKGROUND

At the molecular level, investigations into the mechanism of action of acetylcholine at the neuromuscular junction have focused mainly on a unique neuroeffector junction. This junction is the motor endplate of the electroplax from Electrophorus electricus or the various species of Torpedo and Narcine. Electroplaxes have been studied because of their exceptional richness in nicotinic synapses. Pharmacologically, the electroplaxes respond much like neuromuscular endplates to cholinergic agents and, consequently, are considered to be an excellent model of mammalian nicotinic-neuromuscular synapses [1-3].

Isolated membrane-bound receptors from the electroplax have been shown to undergo multiple conformational changes upon agonist and metaphilic antagonist binding. These transitions have been compared to the transitions between resting and desensitized states, between resting and open channel states, and between open-channel and desensitized states of the endplate observed in vivo. Four sources of evidence have confirmed the existence of these conformational transitions: radioligand binding sites [4], ESR [5], intrinsic fluorescence [6,7] and fluorescence of extrinsic probes [8].

Structure of the Acetylcholine Receptor

The Torpedo californica acetylcholine receptor (AChR) has been the most thoroughly studied of the receptor systems. It is composed of five subunits, two of which two are identical. The subunits are designated α_2, β, γ, and δ and have apparent molecular weights of 40, 49, 58 and 64 K daltons, respectively [9,10]. Only the α-subunits are specifically covalently labeled by affinity reagents such as bromoacetylcholine or 4-(N-maleimido) phenyltri-[^{3}H]-methylammonium iodide (MBTA), suggesting that they contain the acetylcholine binding sites [9,11]. Unlike most other nicotinic receptors, the Torpedo receptor exists primarily as a dimer (70-80%) of disulfide-bonded monomers between the δ-subunits [12]. The dimer can be dissociated into monomers by mild reduction without loss of response to the ionophoretic application of acetylcholine [13]. Each subunit contains carbohydrate moieties which account for 4-7% of their weight [14]. The amino acid sequence indicates significant subunit homology [14-16]. However, peptide maps [17,18] and some lack of immunological cross-reactivity of the subunits [19] indicate some domains of significant differences. In addition to the five subunits of the receptor, there is a base extractable 43 K dalton peptide which associates with the receptor but is not essential for its functional activity [20]. This 43 K dalton peptide appears to be a structural protein which restricts the rotational and translational motions of the receptor [18].

Negatively stained electron micrographs indicate the plasma membrane surface of the Torpedo californica receptor to be disk-shaped, 90 +/- 10A in diameter, with a central cavity of 15-20 A in diameter [21]. The electron density profile through receptor-rich membrane fragments indicates that the receptor extends ~15A into the cytosol with an overall length of ~110A normal to the plane of the membrane [21]. Since all five subunits span the bilayer, it is generally thought that they are like staves in a barrel. The arrange-

ment of the staves appears to be $\alpha\gamma\alpha\beta\delta$ or $\alpha\gamma\alpha\delta\beta$ [7], and a model of the AChR is shown in Fig. 1.

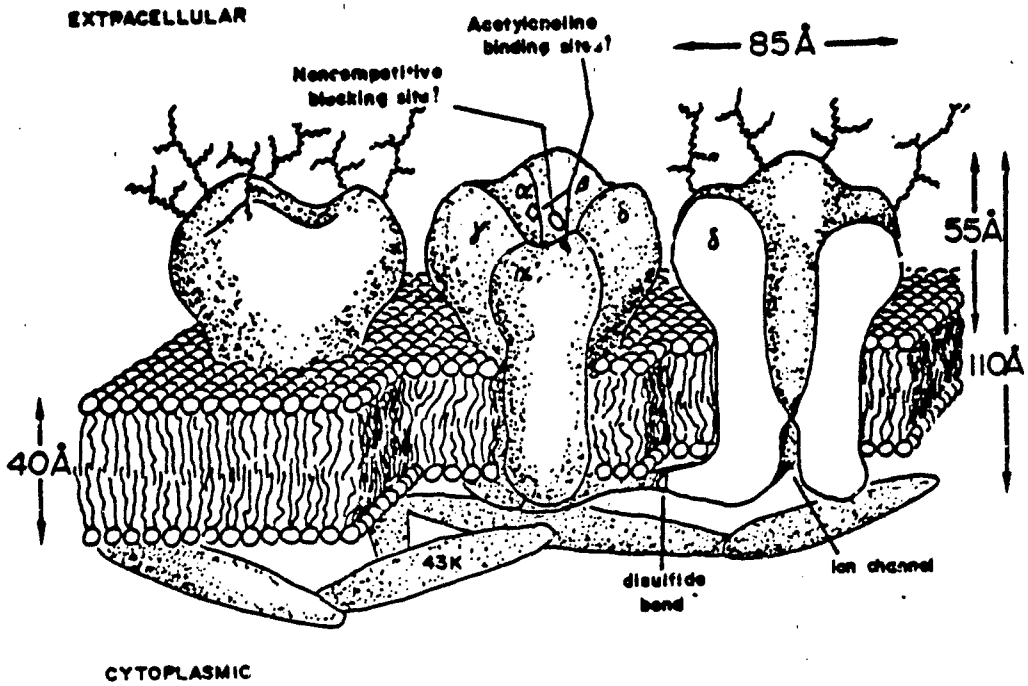

Fig. 1. Model of the acetylcholine receptor.

Ligand Binding Sites on Receptor

Each Torpedo californica receptor contains distinct saturable binding sites or regions of contact for agonists/antagonists [22,23] and for noncompetitive blocking agents [23,25]. While the stoichiometry of α-toxin to noncompetitive binding sites is controversial, variously reported to be four to one [25] or two to one [24], most laboratories agree that there are two agonist/antagonist sites per receptor [2,23,26]. Though binding of agonist, antagonists and snake α-toxins is mutually exclusive and suggestive of common regions of contact on the receptor, important differences exist in the nature of their binding behavior. α-toxins bind independently and with equal affinities to each agonist/antagonist site on the receptor [27]. Classical antagonist binding is characterized by two affinities with equal numbers of sites [28]. For example [^{3}H]d-tubocurarine has dissociation constants of 33 nM and 8 μM [26].

Little is understood concerning the functional activity or the interrelation of subunits. The agonist/antagonist binding sites are located on the α-subunits [9,11]. All five AChR subunits are accessible from either side of the membrane to proteolytic enzymes [29-30] and to antibodies [31-38] and are, therefore, transmembrane polypeptides. α-toxin in the presence of bifunctional reagents will predominately cross-link to the α and δ subunits [30,31], suggesting mutual proximity. Recently, using electron microscopy and single-particle image averaging at 20A resolution, Zingsheim et al. [36] showed that α-bungarotoxin binds to two regions of the receptor. one adjacent to the delta subunit and the other diametrically across the molecule, ~50A away from the δ-subunit. The lipophilic photolabeled [^{3}H]pyrenesulfonyl azide labels primarily the beta and gamma subunits, which suggests that they have pronounced exposure to the membrane lipids [37]. The δ-subunit is affinity-labeled by noncompetitive blockers and a photoaffinity-labeled noncompetitive blocking agent [38], suggesting that it is a site of action of these agents.

Over the last two decades, our understanding of the nicotinic AChR has increased. Two major research areas have been the elucidation of the receptor structure and of ligand modulation of ion permeability. Current work on the receptor structure includes primary amino acid sequencing of the subunits [14-16] and high resolution electron microscopy [19]. The functional responses of interacting ligands are being pursued by now-classical binding methods and electrophysiological techniques. We propose to integrate these disparate approaches by utilizing fluorescence energy transfer [39-41] and quenching techniques [42] as well as peptide mapping and sequencing techniques to examine structural determinants of receptor functional responsiveness. Specifically, we will measure the topographic disposition of fluorescent agonists/antagonists and noncompetitive blocking agents relative to each other and to the surface of the lipid bilayer. The selection of ligands with suitable spectroscopic properties will provide information on the structure and the site of ligand binding as well as information on the pharmacologic selectivity of ligand actions.

The advantages of fluorescence techniques are that (1) only nanomolar concentrations of fluorophores are required, compared to the milli- and micromolar concentrations demanded by other spectroscopic techniques; (2) relatively large fluorophore intersite distances (20-80A) can be measured; and

(3) dynamic measurements can be made on functional molecules, obviating the need for fixatives or frozen preparations dictated by electron microscopy.

The measurement of distances by fluorescence energy transfer techniques requires a detailed knowledge of the spectroscopic and pharmacologic properties of the fluorescent probes. Information return is maximized by use of a variety of donor-acceptor pairs as well as complementary procedures to measure energy transfer, e.g., donor quenching, acceptor sensitization and lifetime analysis.

The goal of this project is to determine the spatial relations between drug binding sites on the surface of the Torpedo AChR and to relate these distances to the primary amino acid sequence of the receptor. This information will provide a connection between current research on the structure of the receptor and that on the functional properties of the receptor-active ligands.

Neuromuscular transmission depends critically upon the interplay between a functionally responsive receptor and rapid inactivation of released acetylcholine by acetylcholinesterase. Conditions of esterase inhibition such as insecticide poisoning lead to acetylcholine accumulation and receptor refractoriness. Better knowledge of drug binding sites can facilitate the design of drugs which mitigate the effects of excess acetylcholine arising from esterase inhibition.

Finally, many diseases affect the neuromuscular junction. In myasthenia gravis, the patient produces antibodies to the AChR. In the case of rabies, the virus appears to enter the nervous system by binding to the AChR [44]. A better knowledge of receptor structure could permit the design of drugs that could block virus or antibody attachment.

Organization of the Report

This report is divided into three sections. Section I deals with our efforts to develop a theoretical framework to analyze solute quenching of fluorescence to determine the solute accessibility of site-specifically labeled α-toxin bound to the surface of the AChR. The solute quenching studies provide information on the disposition of α-toxin on the surface of the AChR. Section II presents our analysis of the interaction of a novel decamethonium homolog, decidium, with the AChR. Section III summarizes our progress to date on site-specifically labeling α-toxin with fluorescein isothiocyanate (FITC), erythrosin isothiocyanate (EITC), and tetramethylrhodamine isothiocyanate (TRITC).

SECTION I

SOLUTE ACCESSIBILITY TO COBRA FLUORESCEIN ISOTHIOCYANATE-N^{ϵ}-LYSINE-23-α-TOXIN BOUND TO THE ACETYLCHOLINE RECEPTOR

Introduction

Solute accessibility to fluorescent probes or groups attached to protein molecules is often used to monitor conformational aspects of these macromolecules. Solute accessibility is most often determined with fluorescence quenchers such as acrylamide and iodide by measuring and comparing the specific rate of quenching of the fluorophore free in solution, k_{FQ}, with its rate attached to the macromolecule, k_{MQ}, or by comparing values of k_{MQ} for two or more conditions that may affect the conformation of the protein. It is usually assumed that a decrease in quenching rate for the bound fluorophore indicates a decreased accessibility due to geometrical masking factors in the macromolecule. However, elementary considerations indicate that for the rapid, diffusion-limited reactions which characterize the fluorescence quenching process, k_{MQ} should depend not only on masking factors but also on the translational and rotational mobilities of the labeled macromolecules as well as on orientational constraints imposed by the association of fluorophores with macromolecules. The lower the rotational mobility, the lower the probability that a bound fluorophore, exposed on a small fraction of the surface area of the macromolecule, will meet a quencher molecule during its excited state lifetime. These notions are supported by recent theoretical formulations on the reactivity of specific groups attached to macromolecules [45-47].

In this section of the report, we establish quantitative relations between the specific rate of quenching, k_{MQ}, translational and rotational mobilities, orientational constraints, and geometrical masking factors, using formulations of Shoup et al. [46]. We then use these relations to analyze iodide quenching data (steady state and time-resolved), which we have measured (a) for fluorescein free in solution, (b) for fluorescein-labeled α-toxin (labeled at lysine 23) free in solution, and (c) for this α-toxin bound to the *Torpedo californica* AChR. The results give information on the extent to which the surface of the α-toxin molecule in the region of lysine 23 is masked when bound to the AChR, and, ultimately, on the disposition of the α-toxin on the surface of the AChR.

Theory

In the fluorescence quenching experiment, the fluorescence intensities of the fluorophore attached to a macromolecule or free in solution are monitored as a function of the quencher concentration. The intensities are then analyzed with the Stern-Volmer equation

$$I_0/I = 1 + K_Q[Q] \qquad (1)$$

where I_o and I are fluorescence intensities observed in the absence and presence, respectively, of a concentration [Q] of quencher. K_Q, the quenching constant, is related to the bimolecular reaction rate, k_{FQ}, by the equation

$$K_Q = k_{FQ}\tau \tag{2}$$

where τ is the fluorescence lifetime. The fundamental parameter for evaluating accessibility is k_{FQ}.

Quenching of Free Fluorophore in Solution. Quenching rate is determined by the rate of encounter between quencher and fluorescent molecule and the probability of reaction per encounter. For the case where the fluorophore, F, and quencher, Q, are spherical molecules, the encounter rate is given by the Fick equation:

$$S = 4\pi R_{FQ}^2 D_{FQ} \partial n_Q(R,t)/\partial R \text{ (molecule/s) (at } R = R_{FQ}) \tag{3}$$

where D_{FQ} is the sum of the translational diffusion coefficients of F and Q. $n_Q(R,t)$ is the average concentration of quencher molecules at a distance R from an excited fluorophore molecule. R_{FQ} is the sum of the molecular radii of F and Q, R_F and R_Q, respectively. The partial derivative is the concentration gradient of quencher molecules about an excited F molecule evaluated at the distance $R = R_{FQ}$. S is essentially the flux due to translational diffusion of quencher molecules across a spherical surface of radius R_{FQ} surrounding an excited molecule and is just the rate of new encounters between F and Q. S is related to k_Q by the equation

$$k_Q = S/n^*_Q \text{ (cm}^3\text{/molecules)} \tag{4}$$

where n^*_Q is the concentration of quencher molecules in the bulk solution. According to theory [47 and 49], when an ensemble of excited molecules is first created by a pulse of light, the quenching rate is initially very high because of encounters between the F and Q molecules that happen to be in close proximity at the time of excitation. However, within 10^{-17} to 10^{-16} s, the system moves to a steady state with a gradient of quencher molecules around each fluorescent molecule. For the case where quenching occurs on every encounter, the specific quenching rate is then given by the Smoluchowski equation (Eq. 5).

$$k_{FQ} = 4\pi D_{FQ} R_{FQ} \tag{5}$$

The interaction of quencher molecules with an excited fluorophore molecule attached to a macromolecule can be considered an asymmetric reaction in which each quencher molecule behaves as a uniformly reactive sphere interacting with a macromolecular sphere that is reactive only on a limited portion of its surface area, as shown in Fig. 2. The reactive area is characterized by the cone angle $2\theta_o$ shown in the figure. For such a reaction, the rate constant depends not only on the collision frequency between quencher and spherical macromolecule (determine by radii and translational diffusion coefficients, as shown by the Smoluchowski equation) but also on the rotational mobility of the macromolecule and θ_o. This is because the number of encounters between macromolecule and its surrounding quencher molecules that are effective at the reactive area depends on the rotational mobility of the macromolecule.

Various authors have offered approximate solutions for this type of reaction, based on considerations of the combined translational and rotational diffusion equations. Here, we follow the solution of Shoup et al. [46] for the analogous reaction. Since the bimolecular reaction rate constant is the quenching rate constant, k_{MQ}, in the steady state, we can evaluate k_{MQ} by Eq. 6 (cf. Eq. 22 in Shoup et al. [46]).

$$k_{MQ} = \frac{8\pi D_{MQ} R^2_{MQ} \kappa (1-\cos\theta_o)^2}{4D_{MQ}(1-\cos\theta_o) - kR_{MQ} \sum_{n=0}} \tag{6}$$

$$\cdot \frac{[P_{n-1}(\cos\theta_o) - P_{n+1}(\cos\theta_o)]^2 K_{n+\frac{1}{2}}(\varepsilon^*_n)}{(n+\frac{1}{2})[(nK_{n+\frac{1}{2}})(\varepsilon^*_n) - \varepsilon^*_n K_{n+3/2}(\varepsilon^*_n)]}$$

where

$$\varepsilon^*_n = R_{MQ}[n(n+1)D_R/D_{MQ}]^{\frac{1}{2}} \tag{7}$$

$D_R(s^{-1})$ is the rotational diffusion coefficient of the macromolecule and κ is a parameter related to the probability of reaction upon encounter. κ approaches a value of infinity for a probability of 1. K is a parameter of a modified spherical Bessel function of the third kind and P_n $(\cos\theta_o)$ is the nth order Legendre polynomial [51].

We use the following procedure to compare our experimental fluorescence quenching data with calculated theoretical rates based on Eq. 6. According to this equation, the quenching rate constant for a fluorescently labeled macromolecule is determined by the values of D_M, D_R, D_Q, R_Q and θ_o. For a spherical protein molecule, D_M, D_R and D_Q can be evaluated from the molecular weight of the protein with Eqs. 10-14 in [52]. Values for D_Q and R_Q can be obtained from the literature. The parameter θ_o can be evaluated as follows. We assume that the fluorophore is treatable as a spherical particle of radius R_F and that the bound fluorophore occupies an area of $4\pi R_F^2$ on the surface of the macromolecule when the fluorophore is fully exposed (completely accessible). The fraction of the protein surface area, F^*_{FM}, occupied by the fully exposed fluorophore is then given by

$$F^*_{FM} = R_F^2/(R_{FM}^2 + R_F^2) \tag{8}$$

For the case where the fluorophore is only partially exposed to the quencher, we let f_{MQ} represent the fraction of the fluorophore's surface area, $4\pi R_F^2$, that is exposed on the surface of the macromolecule. f_{MQ} ranges from 0 to 1 for the completely nonexposed to completely exposed fluorophore and is a measure of quencher accessibility. The fraction of protein surface area occupied by the partially exposed fluorophore is then given by

$$F_{FM} = [f_{MQ}R_F^2/(R_M^2 + f_{MQ}R_F^2)] \tag{9}$$

F_{FM} can thus be evaluated by assigning a value to f_{MQ} and using the values for R_M and R_F obtained as described in the appendix of [50]. Finally, θ_o can be

evaluated with the known equation for the fraction of a sphere's surface area circumscribed by θ_o,

$$\cos \theta_o = 1-2F_{FM} \tag{10}$$

With the procedure described above, we have evaluated k_{MQ} for proteins of different molecular weight and different values of f_{MQ}, assuming a very large value for κ, as is expected for rapid quenching processes that occur in the nanosecond time range. k_{FQ}, the quenching rate constant for the free fluorophore, was calculated with Eq. 5, using $D_F = 4.3 \times 10^{-6}$/sec and $R_F = 5.3A$ for fluorescein. Fig. 3A shows a plot of k_{MQ}/k_{FQ} vs. molecular weight of protein for the fully exposed fluorophore ($f_{MQ} = 1$). Fig. 3B shows plots of k_{MQ}/k_{FQ} vs. f_{MQ} for the partially exposed fluorophore and proteins with molecular weights of 8, 250 and 9,000 kDa. Fig. 3A essentially shows the effects on k_{MQ} of the limited translational and rotational mobility of the macromolecule compared to the free fluorophore, while the plots of Fig. 3B show the additional effects introduced by geometrical masking as measured by f_{MQ}. k_{MQ}/k_{FQ} decreases very rapidly until the mass of the protein reaches about 50 kDa, after which it tends to approach a limit of about 0.38 (Figs. 3A and 2B). According to Fig. 3B, the accessibility parameter, f_{MQ}, is not linearly related to the quenching constant, particular for $f_{MQ} < 0.2$.

Based on the above theoretical calculations, the conjugation of FITC to the α-toxin (8 kDa) should decrease the quenching rate constant, relative to the free fluorophore, by about 39%, while the binding of the labeled α-toxin to the membrane-associated AChR (>>250 kDa) should further reduce the rate constant by about 38%, apart from possible masking effects.

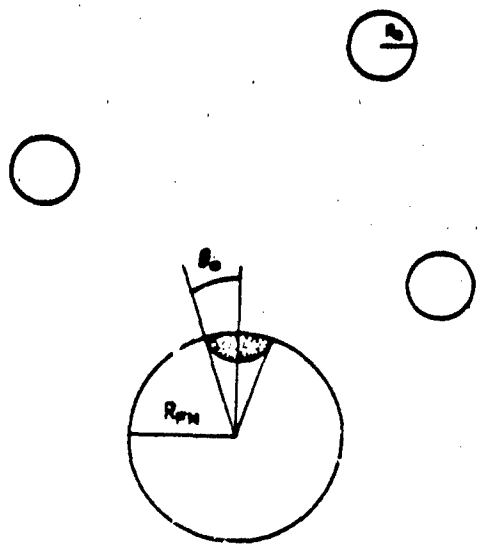

Fig. 2. Model (based on Solc and Stockmaker, [47] and [48] for the interaction of a uniformly reactive quencher with a spherical macromolecule reactive only in an area circumscribed on its surface by a cone drawn from its center with a cone angle of $2\theta_o$. (R_{FM} and R_Q are the radii of the macromolecule and solute, respectively.)

Experimental Procedures

Materials. α-Toxin (siamensis 3) was isolated following the method of Karlsson et al. [52] from Naja naja siamensis venom obtained lyophilized from Miami Serpentarium (Miami, FL). [FITC]-toxin was prepared as described elsewhere [53] and subsequently purified by column isoelectric focusing as described previously [43]. Analytical isoelectric focusing of this material indicated 98% homogeneity based on the distribution of fluorescence. [Mono-^{125}I-tyrosine-25]-α-toxin (siamensis 3) was prepared and separated from noniodinated and diiodo species by column isoelectric focusing [54]. All other reagents were at least reagent grade.

Receptor Isolation. Receptor-rich membrane fragments were isolated from Torpedo californica electric organ following published procedures [55,56]. Aprotin (2.7 trypsin inhibitor units/100 g tissue), phyenylmethyl-sulfonyl-fluoride (0.9 mg/100 g tissue), and EGTA (5 mM) were added during the initial homogenization to minimize proteolysis. The specific binding activities of the receptor preparations were measured by adsorption of [mono-^{125}I]-α-toxin-receptor complexes onto DEAE-cellulose filters [57] and ranged between 1 and 2 nmol of α-toxin binding sites/mg protein. Incubation of tenfold excess of native toxin 30 min prior to the addition of [mono-^{125}I]-α-toxin defined the nonspecific binding component in the total binding.

Fluorescence Lifetime Analysis. Fluorescence lifetimes were determined by the single-photon counting technique, using an EEY scientific nanosecond fluorometer (La Jolla, CA) equipped with a high-pressure hydrogen arc lamp. Data accumulated in a E.G. and G. Ortec 7150 multichannel analyzer (Salem, MA), were analyzed and displayed by using a Compaq computer (Houston, TX) and a Hewlett Packard 7470A plotter (San Diego, CA). Excitation and emission bands were selected with an Oriel 5754 interference filter (Stamford, CT) and a Corning 3-68 cut-off filter (Corning, NY), respectively. Fluorescence decay rates were resolved and assessed as either single or double exponential functions by using the method of moments. The instrumental arrangement and principles of data treatment have been discussed in detail [58,59].

The intensity, I(t), vs. time graph, directly measured with the nanosecond fluorometer, is distorted by the finite duration of the lamp pulse (L(T), and is related to the nondistorted time course of emission (F(t) by the convolution integral (Eq. 11).

$$I(t) = \int_0^t L(T)F(t-T)dT \qquad (11)$$

F(t) was obtained from measured graph of I(t) and L(t) by deconvolution with the method of moments, assuming that F(t) can be represented by a one or two-exponential expression (please see Ref. 56). The time shift between L(t) and I(t) introduced by the spectral response properties of the detecting photomultiplier tube was corrected with a time-shift introduced by the computer. Convolution of F(t) so obtained with L(T) generates a new function, C(t), which can be compared with I(t). The values of coefficients and lifetimes were chosen so that the reduced chi square, x_N^2 was a minimum.

$$x_N^2 = 1/(N-n) \sum (1/\sigma_i^2)[I(t_i)-C(t_i)]^2 \qquad (12)$$

where σ_i is the standard deviation of $I(t_i)$ due to noise, N is the total number of data points and n is the number of parameters being fitted.

Fluorescence Titrations. All steady-state fluorescence measurements were made on a Farrand Mark I spectrofluorometer (Valhalla, NY) equipped with corrected excitation and a Hamamatsu R928 photomultiplier tube (Middlesex, NJ). The spectrofluorometer was interfaced to a Tektronix 4052 microcomputer (Beaverton, OR) via a TransEra analog-to-digital converter (Provo, UT). Samples were maintained at constant temperature in a four-position cell holder turret housed in a water-jacketed sample compartment controlled with a Haake thermostat (Saddle Brook, NJ). Fluorescence titrations were carried out using 1 cm^2 cross-section cuvettes at 20°C. The samples were excited at 480 nm with a Farrand 480 filter in the path of the excitation beam. The emission was monitored at 519 nm with a Corning 3-70 filter in the path of the emission beam. Fluorescence values were corrected for dilution resulting from added titrant, lamp fluctuations, and light scatter. Unless indicated otherwise, all samples were dissolved in 0.1 M NaCl, 10 mM sodium phosphate buffer, pH 7.4, and 0.1 mM sodium thiosulfate to prevent formation of triiodide anion.

Results

Nanosecond Lifetime Determinations. Fluorescence decay rates of [FITC]-toxin free in solution or bound to the AChR reasonably conformed to monoexponential behavior (Figs. 4A and 4B) and were calculated to be 3.9 and 3.8 ns, respectively.

Iodide Quenching. The Stern-Volmer plots for iodide quenching of the fluorescence of fluorescein, [FITC]-toxin in the presence of native α-toxin are shown in Fig. 5. The slopes (K_Q's) of linear least-squares fits to these plots are presented in Table I. Both Stern-Volmer quenching plots of [FITC]-toxin are linear to at least 0.6 M KI (all data not shown) but the fluorescein plot is linear only to about 0.12 M KI. Utilizing Eq. 2 and the measured lifetimes, the quenching rate constants were calculated (Table I). The quenching rate constant of the fluorescein moiety decreased to 45% upon conjugation to the α-toxin and by 80% following binding of the conjugated α-toxin to the receptor.

To assess possible effects of the AChR-associated membranes, iodide quenching of the fluorescence of FITC-toxin in the absence of receptor was determined (data not shown). The Stern-Volmer plots of these titrations yielded quenching constants essentially identical to those observed for FITC-toxin in the presence of native α-toxin-saturated receptor, indicating that the presence of the AChR-associated membrane-induced turbidity did not affect the results.

To assess possible surface charge effects on the negatively charged iodide anion, we measured the quenching constants for samples in 1.0 M instead of 0.1 M NaCl (data not shown). We observed only a slight increase in the quenching rate constants, suggesting that the observed differences are not due to differences in surface charge.

Discussion

In order to obtain information on the disposition of α-toxin bound to the surfaces of the AChR, we determined the solute accessibility to FITC conjugated to N^{ϵ} of lysine-23 of α-toxin bound to AChR. We measured the Stern-Volmer iodide quenching constants and fluorescence lifetimes of the conjugated α-toxin free in solution and AChR-bound and of fluorescein free in solution. From the fluorescence lifetimes and quenching constants, we calculated the bimolecular accessibility. The magnitudes of the quenching rate constants of [FITC]-toxin free in solution and AChR-bound compared to that of fluorescein free in solution were about what would be predicted, if the changes in translational and rotational mobility and orientation constraints were considered. These results strongly suggest that the region about lysine-23 on the α-toxin is exposed to the bulk solvent both when the α-toxin is free in solution and when it is AChR-bound.

Tsetlin *et al.* [60] attempted to determine the solute accessibility to spin-labeled N^{ϵ} on lysine-23 of α-toxin (lysine 27 in their notation) bound to the *Torpedo marmorata* receptor by studying Fe^{3+} and Ni^{2+}-induced paramagnetic broadening. They observed 3- to 5.7-fold higher apparent accessibility to the free α-toxin than to AChR-bound α-toxin. They concluded that lysine-23 is in "contact" with the surface of the receptor. Unfortunately, because they did not measure the paramagnetic broadening of the free toxin in the presence of native α-toxin-blocked receptor, it is not possible to assess the contribution that the presence of the receptor bound to unlabeled α-toxin may have on apparent accessibility. When we attempted to perform the analogous fluorescence quenching experiment with Tl^{+} (data not shown), we observed that the quenching constant of free FITC-toxin was nearly 7 times higher than that of AChR-bound α-toxin. However, in close agreement with our iodide experiments, the quenching constant of FITC-toxin in the presence of carbachol-blocked AChR was about 1.9 times higher than that of AChR-bound FITC-toxin. It is unclear why these differences occurred. Perhaps the AChR altered the chemical potential of the Tl^{+} by nonspecific binding to the negatively charged surface of the AChR.

We have made many assumptions in our calculations of the bimolecular quenching rate constants. Some of these include the spherical shape, the average specific density of all the molecules involved, and the validity of the Stokes-Einstein expression for small molecules such as fluorescein. Thus, we must stress that the predicted quenching rate constants are only first-order approximations. They do show, however, that quenching constants will decrease without an alteration of solute accessibility following binding or conjugation of a small fluorophore to a macromolecule. For the case of FITC-toxin binding to the AChR, there may be a small change in solute accessibility to the FITC associated with AChR binding, but the magnitude is probably small relative to the anticipated effect of AChR-binding.

We are unaware of any other efforts to consider rotational diffusion and orientation constraints on the fluorescence quenching technique. Failure to consider rotation and orientation constraints can potentially lead to problems in the evaluation of accessibility. Two rules of thumb appear to stem from our consideration of rotational diffusion and orientation constraints on fluorescence quenching experiments that involve comparisons between free and bound fluorophores. First, a decrease in the quenching rate constant by a

factor of 2 to perhaps 5 can be expected to occur with the immobilization of a fluorophore on the surface of a macromolecule. Second, the relation between solute exposure and the quenching constant is nonlinear. The nonlinearity of this relation is particularly marked for $f_{FQ} < 0.2$, so that there is no simple direct relation between the fraction of the surface area of the fluorophore exposed to solute and the quenching rate constant (see Fig. 38).

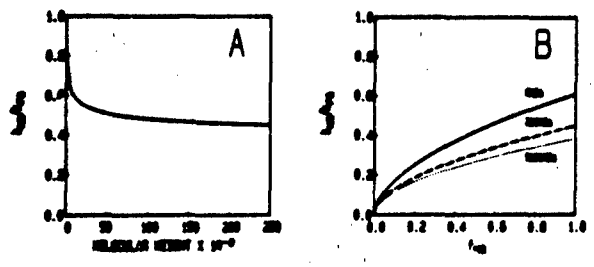

Fig. 3. Theoretical plots based on Eq. 6 of the ratio of iodide ion quenching rate constants for fluorescein bound to a spherical protein (k_{MQ}) and fluorescein free in solution (k_{MQ}) vs. (A) the molecular mass of the protein conjugate, assuming total accessibility of iodide to the fluorophore and (b) the fractional accessibility (f_{MQ}) of iodide to protein-conjugated fluorescein. The fluorophore is assumed spherical with a molecular mass equal to that of FITC (M_r = 389). The lines in panel B correspond to protein molecular masses of 8 kDa, solid line; 250 kDa, dashed line; and 9,000 kDa, dotted line. The radius of the fluorophore was assumed to be 5.3 Å. The translation diffusion rate of fluorescein was estimated to be 4.3×10^{-6} $cm^2 s^{-1}$.

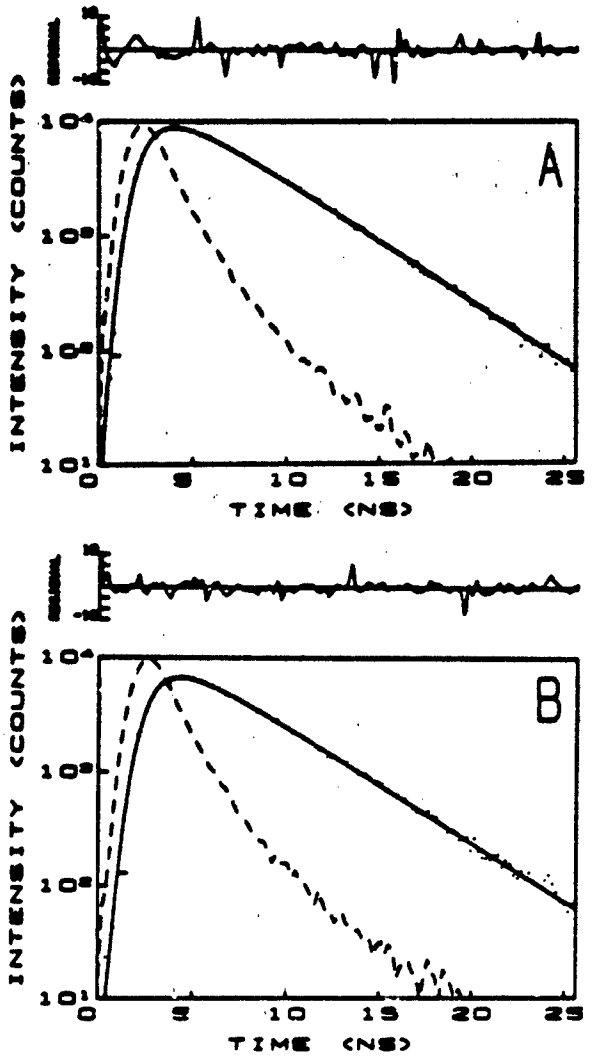

Fig. 4. Nanosecond fluorescence decay curves (A) of [FITC]-toxin (500 nM) bound to the AChR (750 nM in α-toxin sites) and (B) of [FITC]-toxin (500 nM) free in solution in the presence of native α-toxin (4 μM bound AChR). Dashed lines represent lamp pulse. Deviations of the experimental (dotted) from a single exponential theoretical (solid) function are shown in the upper curves. The χ^2_n for the deviation in the upper and lower panels are 1.9 and 1.8, respectively. Native α-toxin was incubated with the receptor 30 min prior to the addition of FITC-toxin.

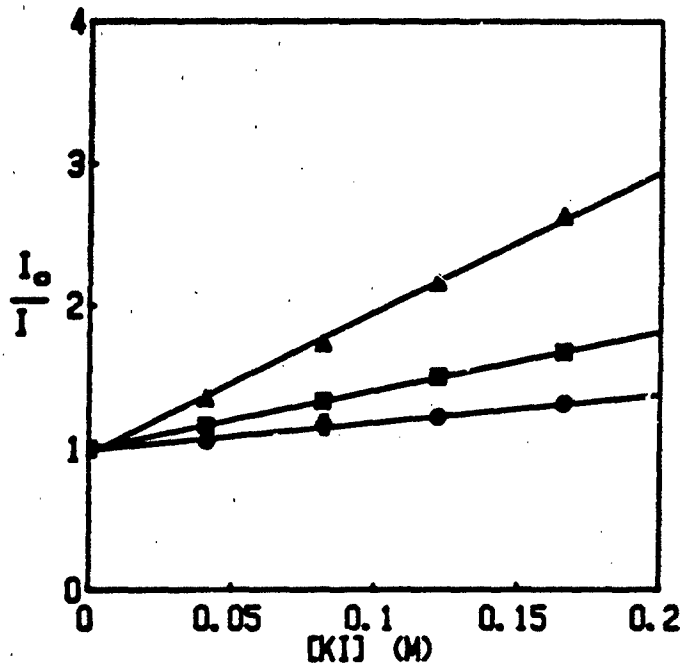

Fig. 5. Stern-Volmer plots of iodide quenching of the fluorescence of fluorescein (triangles), [FITC]-toxin bound to the AChR (circles), and [FITC]-toxin free in a solution containing native α-toxin-saturated AChR (squares). Error bars (n=3) are not shown when they fall within symbol. The concentrations of fluorescein, [FITC]-toxin, AChR and native toxin were 50 nM, 122 nM, 300 nM (in α-toxin sites), and 3 μM, respectively. Native α-toxin was incubated with the receptor for 30 min prior to the addition of FITC-toxin. This mixture was incubated an additional 45 min to ensure that at least 95% of the [FITC]-toxin was bound to the AChR. Solid lines represent linear least-squares fits to the data.

TABLE I. Summary of the Stern-Volmer quenching constants (K_Q) (± standard error of estimate), the fluorescence decay rates (τ), and the bimolecular quenching rate constant (k_Q) of the fluorescein, [FITC]-toxin free in solution (in the presence of toxin-blocked AChR) and bound to the AChR, calculated utilizing Eq. 2. The observed k_{MQ}/k_{FQ} represents the ratio of iodide ion quenching constants for FITC-toxin and free fluorescein. The theoretical k_{MQ}/k_{FQ} values indicate calculated ratios of iodide ion quenching rate constants (Eq. 6/Eq. 5) for a spherical fluorophore the size of fluorescein attached to spherical proteins the size of α-toxin and the AChR relative to the rate constant for the fluorophore free in solution, assuming complete accessibility ($f_{MQ} = 1$).

	$K_Q(M^{-1})$	τ(ns)	$k_Q \times 10^{-9}$ ($M^{-1}s^{-1}$)	Observed k_{MQ}/k_{FQ}	Theoretical k_{MQ}/k_{FQ}
Fluorescein	9.84 ± 0.04	4.1	2.4	1.0	1.0
[FITC]-toxin (plus α-toxin-AChR)	4.07 ± 0.01	3.8	1.07	0.45	0.61
[FITC]-toxin-AChR (membrane-associated)	1.91 ± 0.01	3.9	0.48	0.20	0.38

SECTION II

INTERACTION OF DECIDIUM WITH THE ACETYLCHOLINE RECEPTOR

Introduction

The AChR represents a prototypic transmembrane ligand-regulated ion channel. Coupling of receptor occupation with ion permeability arises from an interplay between interconvertible functional states, modulated by the history of exposure to agonist or a variety of heterotropic ligands, such as phencyclidine (PCP) and local anesthetics. The emerging description of ligand-response coupling reveals a dynamic receptor entity possessing discrete but allosterically interactive sites and functional domains on the receptor oligomer.

Fluorescent ligands containing 5-dimethylaminonaphthalene-1-sulfyl (Dansyl), pyrenebutyl, or 7-nitrobenzo-2-oxa-1,3-diazole moieties have been employed to characterize effector sites and mechanisms underlying functional transitions of the nicotinic receptor. These ligands emit at wavelengths shorter than 550 nm. A ligand which emits at wavelenthgs greater than 600 nm would be useful for assessing intersite distances through excitation energy transfer. To this end, we have characterized the interaction of decidium diiodide with the AChR. Decidium is a fluorescent phenylphenanthridium analogue of ethidium which contains 10 methylene groups between the endocyclic quaternary nitrogen and the exocylic trimethylamino quarternary nitrogen. hence, it contains an interquaternary distance identical to decamethonium and its congeners which have been widely studied in nicotinic receptor function.

In the present study, we described the pharmacological, biochemical and spectroscopic properties of decidium upon interaction with the AChR. Dipolar energy transfer is employed to determine the distance between the two AChR agonist-binding sites using FITC-toxin bound to one and decidium to the other.

To characterize the properties of decidium, we utilized both the BC3H-1 clonal muscle cell line and AChR-enriched membrane fragments from Torpedo californica. BC3H-1 cells grow in monolayer cultures and elaborate uniformly distributed surface AChRs permitting simultaneous measurement of receptor occupation and functional response in the same population of intact cells. Torpedo electric organs provide highly enriched source of receptors for fluorescence measurements.

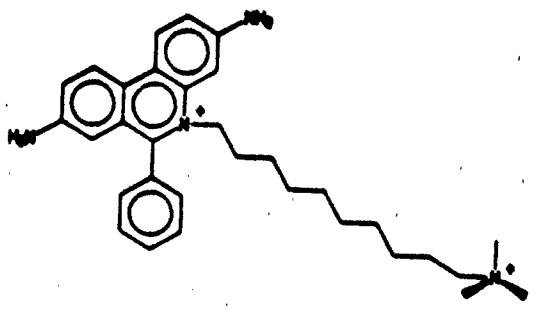

Fig. 6. Structure of the Decidium.

Experimental Procedures

Materials. Cell culture media including Dulbecco's Modified Eagle's Medium and fetal calf serum were obtained from GIBCO (Grand Island, NY). Radionuclides [^{125}I] and $^{22}Na^+$, and [^{3}H]phencyclidine (PCP) were obtained carrier-free from New England Nuclear (Boston, MA). [^{3}H]Acetylcholine (ACh) was purchased from Amersham. PCP was a gift from Dr. Ian Creese. d-Tubocurarine chloride was a gift from Eli Lilly and Company (Indianapolis, IN). Dinapthyl-decamethonium was a gift from Dr. H.P. Rang (Bristol, England). Proadifen was obtained from Smith, Kline, and French (Philadelphia, PA). Meproadifen was prepared by methylating proadifen with iodomethane. Lidocaine and carbachol were from Sigma Chemical Co. (St. Louis, MO). Decidium was synthesized by Dr. Harvey Berman. Stock decidium solutions were freshly prepared by dissolving a small amount of dry decidium directly into aqueous buffer. The solution was clarified by filtration and the decidium concentration determined from the absorbance at 480 nm (E_{480} = 6000 M^{-1} cm^{-1}). Alternatively, concentrated decidium solutions were prepared in acetonitrile and stored, protected from light, at -20°C. Experimental solutions were freshly prepared by dilution of the concentrated stock into aqueous buffer. FITC-toxin was prepared as described elsewhere [43] and subsequently purified by column isoelectric focusing as described previously [52]. Analytical isoelectric focusing of this material indicated 98% homogeneity based on the distribution of fluorescence. α-Toxin (siamensis 3) was isolated following the method of Karlsson et al. [52] from Naja naja siamensis venom obtained lyophilized from Miami Serpentarium (Salt Lake City, UT). [Mono-^{125}I-tyrosine-25]-α-toxin (siamensis 3) was prepared and separated from noniodinated and diiodo species by column isoelectric focusing [53]. All other reagents were at least reagent grade.

Receptor Isolation. Receptor-rich membrane fragments were isolated from Torpedo californica electric organ as described in Section I.

Assays of receptor occupation and agonist-stimulated permeability response. Kinetic assays to measure ligand competition with the initial rate of [^{125}I]-α-toxin binding to AChR in Torpedo membranes were performed using Whatman DE-81 filter discs to adsorb selectively the receptor-toxin complex as described previously [55]. Filters were acid washed prior to experiments in order to reduce nonspecific adsorption of [mono-^{125}I]-α-toxin to the filters. They were acid-washed prior to experiments as follows. Batches of 50-100 filters were suspended in a solution of 12 ml concentrated HCl plus 28 ml methanol, warmed to 43°C, and allowed to cool to room temperature over ~45 min. The solution was decanted and the filters were washed twice with distilled water, soaked overnight in a further rinse of distilled water, and then dried under a heat lamp before use.

Assays of ligand competition with initial rates of [^{125}I]-α-toxin binding and agonist-stimulated $^{22}Na^+$ permeability in intact BC3H-1 cells were performed as described previously [27,28].

[^{3}H]PCP Binding. The equilibrium binding of radiolabeled PCP was measured as described by Heidemann et al. [61] with the following modifications: AChR-associated membranes were suspended in 100 mM NaCl, 10 mM $NaPO_4$, pH 7.4. Binding of [^{3}H]PCP was determined under the following conditions: 1) Membranes were not treated with any cholinergic ligand prior to [^{3}H]PCP addition;

2) a 10-fold excess of α-toxin was incubated with AChR for 1 hr prior to addition of [^{3}H]PCP; and 3) 200 μM carbachol was incubated with AChR for at least 10 min prior to the addition of [^{3}H]PCP. Nonspecific binding was determined by the level of [^{3}H]PCP binding in the presence of 1 mM PCP. A 20 μM [^{3}H]PCP stock solution was prepared so that the final concentration of [^{3}H]PCP in the samples was 1.0 μM. After addition of the noncompetitive inhibitor ligand, the samples were incubated for at least 1 hr at 20°C in Beckman polyallomer airfuge tubes. Bound ligand was separated from free ligand by ultracentrifugation in a Beckman Airfuge for 5 min at 160,000 x g. For Scatchard analysis, duplicate 10 μL aliquots of the supernatant were removed, or alternatively, aliquots were withdrawn prior to centrifugation to determine total counts. The supernatant was then aspirated, and 3 mm of the end of the tube containing the pellet was cut off. The membrane pellets and supernatant aliquots were counted in 5 mL of Biofluor (New England Nuclear, Boston, MA).

[^{3}H]ACh Binding. The binding of [^{3}H]ACh to Torpedo membranes was measured in 100 mM NaCl, 100 mM $NaPO_4$, pH 7.4 by an ultracentrifugation assay. In order to prevent catalytic ACh hydrolysis, AChR-associated membranes (2.5 μM in α-toxin sites) were incubated with 1 mM diisopropylfluorophosphate for 1 hr at 25°C. Binding studies were subsequently made in the presence of 10 μM diisopropylfluorophosphate, AChR-associated membranes (<5 nM in α-toxin sites, and [^{3}H]ACh (20 nM). Incubations were performed in the presence and absence of noncompetitive inhibitor ligands for 1 hr at 25°C. Nonspecific binding was determined by pre-incubating the AChR-associated membranes with 10-fold excess α-toxin for 1 hr. After ultracentrifugation in a Beckman Airfuge for 5 min at 160,000 x g, the supernatant was aspirated. The pellet was then solubilized by addition of 30 μL 10% (w/v) Triton X-100 for at least 18 hr. The radioactivity was counted in 5 mL of Biofluor.

Binding Data Analysis. Competition binding experiments were analyzed by the LIGAND nonlinear curve fitting program for the analysis of ligand binding data, model fitting and parameter estimation.

In order for the program to calculate the K_D of the unlabeled competitor, a value for the K_D of [^{3}H]PCP had to be determined. Since the K_D of [^{3}H]PCP is allosterically modulated by binding at the agonist/antagonist sites, we determined K_D values of 0.4 μM and 2.0 μM in the presence of carbachol and α-toxin, respectively. The data points are the means of duplicate samples. Scatchard plots were fit by least-squares linear regression analysis. Figures show the results of individual experiments, each of which was performed at least three times with different membrane preparations.

Fluorescence Lifetime Analysis. Fluorescence lifetimes were determined by single-photon counting technique using an EEY scientific nanosecond fluorometer as described in Section I.

Energy Transfer. The efficiency of dipolar resonance energy transfer between a discrete donor and acceptor pair is related to the distance (R) separating the pair by Equation 13.

$$R = R_0(1/E - 1)^{1/6} \qquad (13)$$

R_0, the distance at which transfer efficiency equals 50%, is $9.756 \times 10^3 (\kappa^2 J Q_D \eta^{-4})^{1/6}$. The overlap integral, J, between excited state donor and acceptor dipoles is the integrated area of overlap between the donor emission spectrum, $I_D(\lambda)$, and the acceptor absorption spectrum, $\epsilon_A(\lambda)$ (Equation 13).

$$J = \frac{\int I_D(\lambda)\epsilon_A(\lambda)\lambda^4 d\lambda}{\int I_D(\lambda)d\lambda} \tag{14}$$

Q_D denotes the donor quantum yield in the absence of acceptor and η represents the refractive index of the medium between donor and acceptor. κ^2, the orientation factor, accounts for the relative orientation of the donor emission and acceptor absorption transition dipoles. λ is the wavelength in cm.

When donor and acceptor are at separate sites on a macromolecule, the efficiency of energy transfer (E_D) can be measured by

$$E_D = 1 - \tau_{DA}/\tau_D \tag{15}$$

where τ_{DA} and τ_D are the fluorescence lifetimes of the donor in the presence and absence of acceptor, respectively.

The distance relationships between FITC-toxin and decidium bound to the agonist sites on the AChR was examined after 15% of the agonist sites were occupied with the FITC-toxin. This value was chosen as a compromise between maximizing the signal from FITC-toxin while minimizing the number of receptors with both agonist sites occupied with FITC-toxin. Since FITC-toxin binds with equal probability to either of the two agonist sites, the formula for a binomial distribution was used to estimate the proportion of doubly versus singly occupied receptors. With 15% of all the α-toxin binding sites occupied by [FITC]-toxin, 82% of the [FITC]-toxin occupied receptors will have only one toxin molecule bound, and 17% will have two FITC-toxin molecules bound (cf. Table I in 63). After the [FITC]-toxin was incubated with the AChR, the remaining unoccupied sites were occupied by a near saturating concentration of decidium, 10 μm. PCP (100 μm) was present to prevent decidium binding to the noncompetitive inhibitor site.

Results

Concentration dependence for decidium inhibition of initial rates of [^{125}I]-α-toxin binding and agonist-stimulated $^{22}Na^+$ permeability. In order to assess the utility of decidium as a fluorescent probe of AChR, it was first necessary to characterize the pharmacological actions of the ligand. Since classical agonists and antagonists competitively inhibit α-toxin binding to the receptor, decidium was tested for concentration-dependent inhibition of the initial rate of [mono-^{125}I]-α-toxin binding. In addition, the decidium concentration dependence for inhibition of the initial rate of $^{22}Na^+$ influx stimulated by carbachol was examined. Data are shown in Fig. 5. Decidium inhibits α-toxin binding to AChR in Torpedo membranes (Fig. 7A) and in intact BC3H-1 cells over similar concentration ranges. Decidium also effectively inhibits the $^{22}Na^+$ influx stimulated by carbachol in BC3H-1 cells over a comparable concentration range, suggesting that the two effects might be mediated through action at the agonist/antagonist site. In control

experiments, decidium alone causes no detectable increase over basal $^{22}Na^+$ permeability (data not shown). As previously noted with a variety of cholinergic antagonists [28], the decidium protection curves in Fig. 7C show Hill coefficients of less than unity. This behavior may arise from heterogeneity in decidium affinities for the two agonist/antagonist subsites on the AChR macromolecule. It is interesting that equilibration of AChR with the specified decidium concentrations prior to initial rate measurements in the continued presence of decidium (Fig. 7, closed symbols) resulted in a small increase (approximately 3-fold) in decidium affinity relative to that for decidium added to AChR during the initial rate measurement without prior exposure (Fig. 7, open symbols). This observation suggests that in addition to its antagonist actions on AChR, decidium may possess limited ability to convert AChR to a desensitized state exhibiting increased affinity for this ligand. Such a conversion in AChR state might occur through the action of decidium at the agonist/antagonist site as a metaphilic antagonist as described by Rang and Ritter [57] or by an additional component of decidium action as an allosteric inhibitor like the local anesthetics.

Decidium Inhibition of Concentration-Dependent Agonist Activation of AChR Permeability Response. In order to examine further the mechanism of decidium inhibition of AChR function, the concentration dependence for carbachol activation of $^{22}Na^+$ permeability response was measured in BC3H-1 cells in the presence of fixed concentrations of decidium. As shown in Fig. 8A, increasing decidium concentrations progressively displaced the carbachol concentration-response curve to higher agonist concentrations as well as reduced the maximal response obtained at saturating agonist concentrations. This experiment reveals both competitive and noncompetitive components of decidium inhibition. For comparison, Fig. 8C shows the effect of the competitive antagonist d-tubocurarine. As expected, this antagonist shifted the agonist concentration-response curve to higher concentrations without altering the maximal obtainable permeability response. Fig. 8B illustrates the behavior of the metaphilic antagonist dinapthyldecamethonium. Like decidium, dinapthyldecamethonium displayed substantial noncompetitive inhibition, consistent with conversion of AChR to a desensitized state temporarily incapable of responding to agonist.

Decidium Enhancement of Agonist Competition with α-toxin Binding. The data in Figures 7 and 8 do not distinguish between actions at the agonist/antagonist site and anesthetic-like actions at additional allosteric sites as the mechanism by which decidium converts AChR to a state of increased affinity and decreased functional responsiveness. If decidium's actions were exerted solely through the agonist/antagonist site, any effect of decidium to enhance the apparent agonist affinity should occur over the same concentration range at which decidium itself competes with [mono-^{125}I]-α-toxin binding. Alternatively, if decidium could convert AChR to a state of increased agonist affinity by an allosteric mechanism, as demonstrated for the local anesthetics, one might observe a separation between the concentration dependences for direct decidium competition versus indirect enhancement of agonist competition with α-toxin binding [59]. To address this question, we examined the concentration dependences for decidium augments competition of a fixed agonist concentration with the initial rate of [mono-^{125}I]-α-toxin binding in the absence of carbacholine. Results from experiments in Torpedo membranes and BC3H-1 cells are shown in Figs. 9A and 9B, respectively. These data show that decidium exhibits identical concentration dependences for inhibition of α-

toxin binding and for augmentation of the competition of carbachol with α-toxin binding. Fig. 9C shows the corresponding result obtained for the local anesthetic meproadifen with Torpedo membranes. Here meproadifen allosterically enhances carbachol competition with α-toxin binding at far lower concentrations than those required for inhibition of α-toxin binding by the anesthetic itself.

Decidium Inhibition of [^{3}H] ACh Binding. To further confirm and analyze the interaction of decidium with the agonist/antagonist site, we measured the concentration dependence of decidium inhibition of [^{3}H] binding to the Torpedo membranes at equilibrium. Fig. 10A shows a plot of the percent inhibition of [^{3}H]ACh binding as a function of decidium concentration. In close agreement with the above α-toxin binding inhibition studies, the calculated inhibition constant of decidium was about 0.4 μM.

Decidium Inhibition of [^{3}H]PCP Binding. To measure directly the interaction of decidium with the noncompetitive binding site, we examined the capacity of decidium to inhibit the equilibrium binding of [^{3}H]PCP to Torpedo membranes. PCP had been shown to bind selectively to the noncompetitive blocking site [61]. Fig. 10B shows the concentration-dependent inhibition of [^{3}H]PCP binding in the presence of excess carbachol or α-toxin to block the binding to the agonist/antagonist sites and in the absence of both agents. Since a nonsaturating concentration of [^{3}H]PCP was utilized, it was possible to observe about a 100% increase in [^{3}H]PCP binding in the presence of carbachol compared with α-toxin. Moreover, PCP has about fourfold higher affinity toward the carbachol-induced high affinity state (K_D = 4.8 μM) compared to the α-toxin-stabilized state (K_D = 18.2 μM). In the absence of either carbachol or α-toxin, decidium displays biphasic behavior. At low concentrations, decidium increases PCP binding and at high concentrations, it inhibits binding. This biphasic behavior is consistent with decidium's higher affinity toward the agonist-induced high affinity state. Decidium, which binds at tenfold lower concentration to the angonist/antagonist site than to the noncompetitive blocking site, converts the receptor to the high affinity state, which increases the apparent affinity of PCP and, in turn, the fraction of occupied PCP sites.

Spectral Characterization. By measuring the fluorescence spectra of decidium in the presence of various combinations of excess carbachol and PCP, it is possible to block selectively the binding of decidium to either the agonist/antagonist or noncompetitive blocking sites on the surface of the receptor, and thereby obtain the spectra of decidium bound to each binding site. Fig. 11 shows that the excitation spectrum of decidium bound to the spectrum of decidium bound the agonist/antagonist site. This blue shift may reflect an interaction of the aromatic protion of decidium with a charged group in the noncompetitive blocking site between the emission spectra not in the agonist/antagonist site. Fig. 12 shows no difference of decidium bound to either of the two types of binding sites.

Prior to performing any energy transfer studies with decidium and FITC-toxin, the spectral relationship for energy transfer between [FITC-lys-23]-toxin as donor and decidium as acceptor had to be determined. This relationship is shown in Fig. 11. The spectral overlap integral is 2.49 x 10^{-14} $cm^3 \cdot M^{-1}$. Assuming a standard refractive index for proteins of 1.4 and an

orientation factor (κ^2) of 0.67, the distance at which energy transfer would be 50% is 30 A.

Energy Transfer Between FITC-toxin and Decidium. To examine the distance between the two agonist sites on the individual receptor molecules, we assessed dipolar fluorescence energy transfer between FITC-toxin and decidium bound to the agonist sites on the receptor. Doubly liganded receptors were prepared to achieve the fractional occupation described under "Experimental Procedures." Saturating concentrations of PCP were added to prevent decidium binding to the noncompetitive inhibitor site. The spectral overlap integral between FITC emission and decidium excitation, J, was calculated to be 2.40 x 10^{-14} $cm^3 \cdot M^{-1}$ (cf. Fig. 13 and data not shown). Assuming a refractive index of 1.4 and an orientation factor (κ^2) of 0.67, R_0 was calculated to be 30 A.

Various factors render quantitation of steady-state energy transfer between FITC-toxin and decidium bound to the AChR difficult. These factors include the significant overlap of decidium and FITC emission spectra and the inner filter effects of decidium at the FITC absorption maxima. Since fluorescence lifetimes are unaffected by inner filter effects and since an appropriate combination of interference filters could be chosen which reduces the contribution of decidium fluorescence to less than 5% of the FITC fluorescence signal, we have chosen to determine energy transfer as the extent of reduction of donor FITC fluorescence lifetime (Equation 15) in the presence of the acceptor decidium. The results of studies on membrane-associated and detergent-solubilized receptor preparations are presented in Table II. In the absence of added decidium and with 15% occupancy by FITC-toxin, the exponential decay of FITC-toxin fluorescence was satisfactorily described by a single fluorescence lifetime (τ = 3.9 ns). When decidium was added to saturate the remaining agonist sites, a 16% decrease was observed in the fluorescence lifetime of FITC-toxin bound to the membrane-associated AChR. This quenching was not altered by the further addition of native α-toxin and was abolished by solubilizing the receptor with cholate. Taken together, the reduction in FITC-toxin fluorescence lifetime does not stem from decidium at the agonist site or nonspecifically associated with the receptor molecule but reflects energy transfer between FITC-toxin bound to the agonist site and decidium partitioned nonspecifically into the lipid bilayer. If we assume a detection limit of 5% transfer between agonist sites, then Equation 12 predicts a minimum separation between fluorophores at the agonist sites of 1.63 x R_0 or 49 A. Hence, the greater than 49 A separation between the agonist sites is too distant to produce the reduction in lifetime of FITC-labeled toxin in the presence of decidium. The minimal but measurable excitation transfer efficiency indicates that at high concentrations decidium can partition into the membrane.

Discussion

The dynamics of the nicotinic AChR function have been extensively studied from several perspectives [2,3]. Within the timescale in which our studies are conducted, the AChR can be thought to exist in equilibrium between at least three types of states: resting (R), activated (R*), and desensitized (R'). Additional transient desensitized states have been shown to exist but after equilibrium exposure a single desensitized state is presumed to predominate.

Changes in the population distribution of receptor molecules between these states govern the functional and binding properties of the receptor. In the absence of agonist (L) or noncompetitive inhibitor (A), the receptor exists predominantly in the activatable state (RR), exhibiting a comparatively low agonist affinity. Agonists bind to receptor, activate the cation channel, and concomitantly but more slowly convert the receptor to a desensitized state. The desensitized states display higher agonist binding affinity and no receptor-mediated cation permeability. The preference of a ligand for binding to the desensitized receptor is the driving force underlying desensitization.

Agents which perturb receptor functional responses may do so by competitive or noncompetitive mechanisms. Classical antagonists inhibit agonist-stimulated cation fluxes by direct competition at the agonist-binding sites [26], exhibit little or no preference for the R'R' relative to RR states and do net effect transitions to the active state [28]. A large and heterogeneous class of inhibitors noncompetitively inhibit channel opening by agonists. Most, but not all, of these noncompetitive inhibitors enhance the conversion of receptor to a desensitized state. Typical of such agents are the local anesthetics, general anesthetics, PCP, and certain toxins such as histrionicotoxin. Certain antagonists competitively inhibit agonist activation and in addition convert the receptor to a desensitized state. Classical pharmacolo-

gic studies distinguish these agents as metaphilic antagonists [58]. Metaphilic antagonists exhibit higher affinity for the desensitized state of the receptor and therefore show a greater capacity to block the permeability response after exposure to carbachol. The actions of decidium are consistent with it exhibiting metaphilic properties. Decidium exhibits mixed competitive and noncompetitive inhibition of agonist-stimulated $^{22}Na^+$ influx (Fig. 9). Equilibrium exposure of the receptor to decidium converts the receptor to a state exhibiting increased decidium binding affinity (Fig. 10). Decidium binding to the agonist site enhances [^{3}H]PCP binding to an allosterically coupled noncompetitive site (Fig. 8B). Decidium by itself does not stimulate $^{22}Na^+$ influx in BC3H-1 cells, so it is not a partial agonist. Hence, these results indicate that upon occupation of the agonist sites decidium converts the AChR to a functionally blocked state toward which agonists and noncompetitive inhibitors display a higher affinity. In addition to its functional antagonism, and ability to convert the receptor to a high affinity state by occupying the agonist sites, decidium at higher concentrations binds directly to the PCP-binding site (Fig. 10B).

Fluorescence characterization of decidium bound to the two classes of binding sites indicates significant shifts in both the excitation and emission spectra, which are consistent with an environment of greater hydrophobicity upon binding to the AChR. A red-shift in the excitation spectrum of far greater magnitude is associated with decidium binding to the noncompetitive site (~50 nm) than to the agonist sites (~10 nm). This suggests that the noncompetitive site for PCP is more hydrophobic than the agonist-binding sites, i.e. in a domain less susceptible to solvent proton transfer from the excited singlet state.

In a previous study of the interaction of ethidium with the AChR, we observed that this phenylphenanthridium ligand binds selectively to the noncompetitive inhibitor site for PCP, particularly when the receptor is in a desensitized state (K_d ~0.4 μM) [62]. Like decidium, ethidium displays a large red-shift in the excitation (~47 nm) and a blue-shift in the emission (~35 nm) maxima upon binding to the noncompetitive inhibitor site for PCP. These results also show that a portion of the binding domain of the noncompetitive site is particularly hydrophobic. Furthermore, addition of a second quaternary group separated by 10 methylene groups dramatically changes the relative binding selectivity of these phenylphenanthridium congeners for the two respective sites.

Fluorescence titrations confirm that functional antagonism by low concentrations of decidium occurs via occupation of the agonist site and that decidium binds nonequivalently to the two agonist sites on the receptor oligomer, although the degree of nonequivalence is small relative to antagonists such as pancuronium or dimethyl-d-tubocurarine. Studies on reversible [26,28,53] and site-directed irreversible antagonists [63] also show nonequivalence of the sites. Despite the identity in the sequence of the α subunits [14] differential post-translational glycosylation has been reported. Thus, either the differential glycosylation or the lack of identity of subunits neighboring the α-subunit could be responsible for the nonequivalence in binding sites.

To measure distances between the two agonist sites on the receptor, we estimated the efficiency of excitation energy transfer between a slowly

reversible α-toxin and a highly reversible ligand, decidium. We observed no energy transfer between the FITC-toxin and the decidium when each is bound to one of the two agonist sites on doubly liganded receptors. Previous studies using a hybrid receptor-fluorescent-α-toxin complex, where FITC-toxin is on one of the subunits and tetramethylrhodamine-toxin occupies the other subunit, exhibit intersubunit and interreceptor transfer in the membrane-associated receptor and intersubunit transfer in the solubilized receptor. Intersubunit excitation transfer measurements afforded a distance of 67 A (range 55-85 A) between the fluorophores conjugated to lysine 23 of the α-toxin, consistent with location of these lysine 23-conjugated fluorophores at the outer perimeter of the 85-90 A diameter receptor molecule. However, interpretation of these data was limited by uncertainty in the location of the fluorophore relative to the orientation of bound α-toxin molecule. Although the α-carbon of lysine 23 is no more than 19 A away from any other α-carbon in the α-toxin, the α-toxin molecule is an asymmetric, peptide (M_r = 7820) with dimensions of 20 x 30 x 40 A. The absence of energy transfer between lysine 23-FITC-toxin and decidium in the present study confirms our previous estimate of the intersite distance measured between fluorophores conjugated at lysine 23 on the two α-toxin molecules. With a critical transfer distance of 30 A for fluorescein to decidium, 5% transfer of energy will occur at 49 A. This value is significantly less than the 67 A measured between fluorophores for the two fluorescent α-toxins. If the agonist sites where decidium binds are located on the extracellular surface near the pseudo-axis of symmetry, then energy transfer should have been observed. The absence of detectable energy transfer confirms our previous suggestion that the agonist sites reside at a distance from rather than near the pseudo-axis of symmetry of the receptor. Our findings are consistent with previous suggestions that the central loop of the α-toxin, which contains lysine 23, overlies the agonist site. Thus, energy transfer studies with decidium have allowed us to place further constraints on the location of the agonist sites when ligands are associated with the receptor.

While no site-specific energy transfer was detected between the decidium and FITC-toxin specifically bound to the agonist sites, minimal dipolar transfer efficiency (16%) can be detected between FITC-toxin and decidium associated nonspecifically with the lipid or the receptor molecule. Decidium has sufficient hydrophobicity to partition into the lipid bilayer. Since we also found no energy transfer with the solubilized receptor, the membrane itself is the likely site of nonspecific decidium association. Due to uncertainty in the donor-acceptor stoichiometry, precise estimates of distance between the agonist site and lipid bilayer cannot be obtained. Nevertheless, our results suggest proximity of the agonist-binding sites to the lipid bilayer, which is consistent with the recent finding of the Cys-192 and Cys-193 are proximal to both the acetylcholine-binding site and the beginning of the proposed M1 membrane spanning hydrophobic region (Ile-210) of the α subunit.

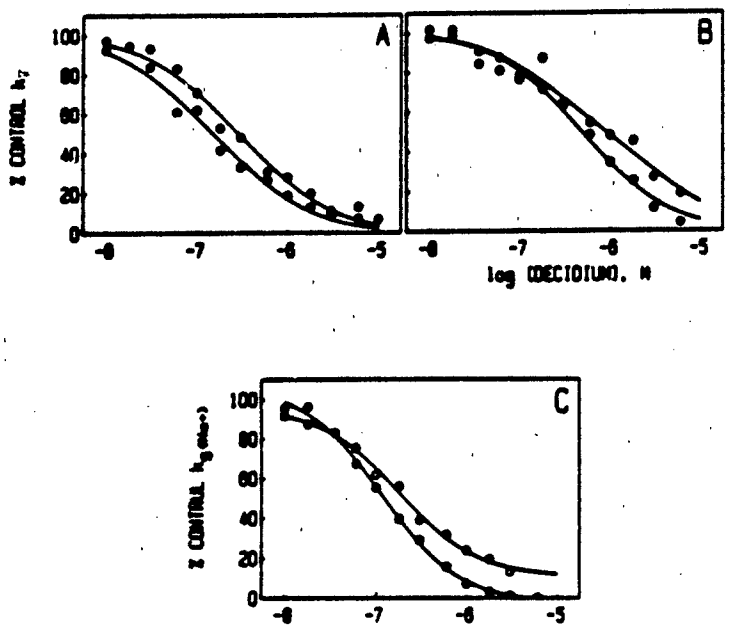

Fig. 7. Concentration-dependent decidium inhibition of initial rates of cobra [^{125}I]-α-toxin and carbachol-stimulated $^{22}Na^+$ influx in Torpedo membranes and BC3H-1 cells. Initial rates of α-toxin binding to AChR in Torpedo membrane fragments (A) or monolayer BC3H-1 cultures (B) were measured in the presence of the indicated decidium concentration. Data were normalized to the rate of α-toxin binding the absence of decidium. Initial rates of carbachol-stimulated $^{22}Na^+$ influx were measured in BC3H-1 cells (C) in the presence of 60 μM carbachol plus the indicated decidium concentrations. Data were normalized to the rate of α-toxin binding in the absence of decidium. Initial rates of carbachol-stimulated $^{22}Na^+$ influx were measured in BC3H-1 cells (C) in the presence of 60 μM carbachol plus the indicated decidium concentrations as described in Experimental Procedures. Data were normalized to the agonist-stimulated $^{22}Na^+$ influx observed in the absence of decidium. Experimental determinations were routinely made in duplicate. ●-●, Equilibrium exposure to buffer containing the indicated decidium concentrations followed by initial rate measurements in the presence of decidium plus carbachol. o-o, Equilibrium exposure to buffer alone followed by initial rate measurements in the presence of the indicated decidium concentrations.

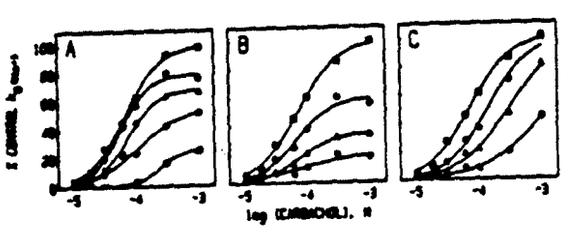

Fig. 8. Antagonist inhibition of concentration-dependent carbachol activation of receptor permeability response in BC3H-1 cells. Sets of cultures were equilibrated with physiological buffer; then the $^{22}Na^{+}$ permeability response was measured in response to the specified concentrations of carbachol plus antagonist over a 20 s interval. Results are expressed as percent of the maximum rate in the absence of antagonist. (A) Decidium: ■-■, no added decidium; ●-●, 10^{-7}; ▲-▲, 3×10^{-7} M; o-o, 10^{-6} M; □-□, 3×10^{-6} M. (B) Dinapthyldecamethonium: ■-■, no added dinapthyldecamethonium; ●-●, 6×10^{-7} M; ▲-▲, 3×10^{-6} M; o-o, 10^{-5} M. (C) d-Tubocurarine: ■-■, no added d-tubocurarine; ●-●, 3×10^{-7} M; ▲-▲, 10^{-6} M; o-o, 6×10^{-6} M.

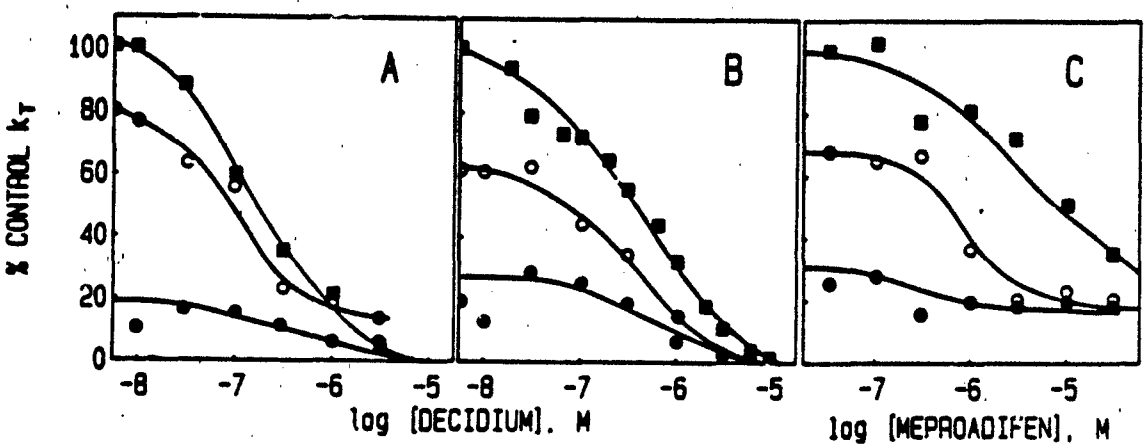

Fig. 9. Decidium and meproadifen enhancement of carbachol competition with the initial rate of [^{125}I]-α-toxin binding to AChR in Torpedo membranes and BC3H-1 cells. Decidium and meproadifen in the specified concentrations are added 30 min prior to initiating the toxin-binding reaction. Carbachol is added either 10 or 30 min prior to addition of α-toxin. Initial rates of toxin binding are measured for the first 40 min of the reaction as a percent of the rate observed in the absence of carbachol, decidium, or meproadifen. o-o, Rate of binding measured with 10 s of prior exposure to agonist; ●-●, rate of binding with 30 min of prior exposure to agonist; ■-■, rate of binding with exposure only to decidium or meproadifen. (A) decidium, Torpedo membranes: The test carbachol concentration was 1 μM. (B) Decidium, BC3H-I cells: The test carbachol concentration was 30 μM. (C) Meproadifen, Torpedo membranes: The test carbachol concentration was 1 μM, as in panel A.

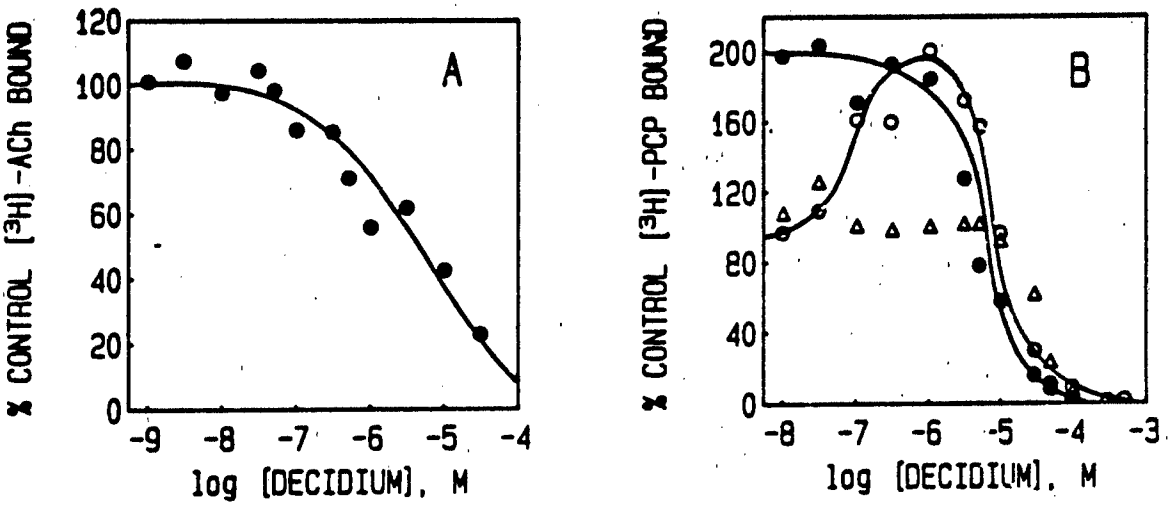

Fig. 10. Decidium inhibition of [^{3}H]acetylcholine and [^{3}H]PCP binding to the Torpedo membranes. A. Inhibition of [^{3}H]acetylcholine (50 nM) binding to AChR membranes (50 nM in α-toxin sites). B. Inhibition of [^{3}H]PCP (1 μM) binding to Torpedo membranes (1 μM in α-toxin sites: ●-●, in the presence of carbachol (200 μM); Δ-Δ, in the presence of α-toxin (10 μM); o-o, in the absence of either α-toxin or carbachol. Carbachol, α-toxin, and decidium were added 10 min prior to the addition of [^{3}]acetylcholine to [^{3}H]PCP.

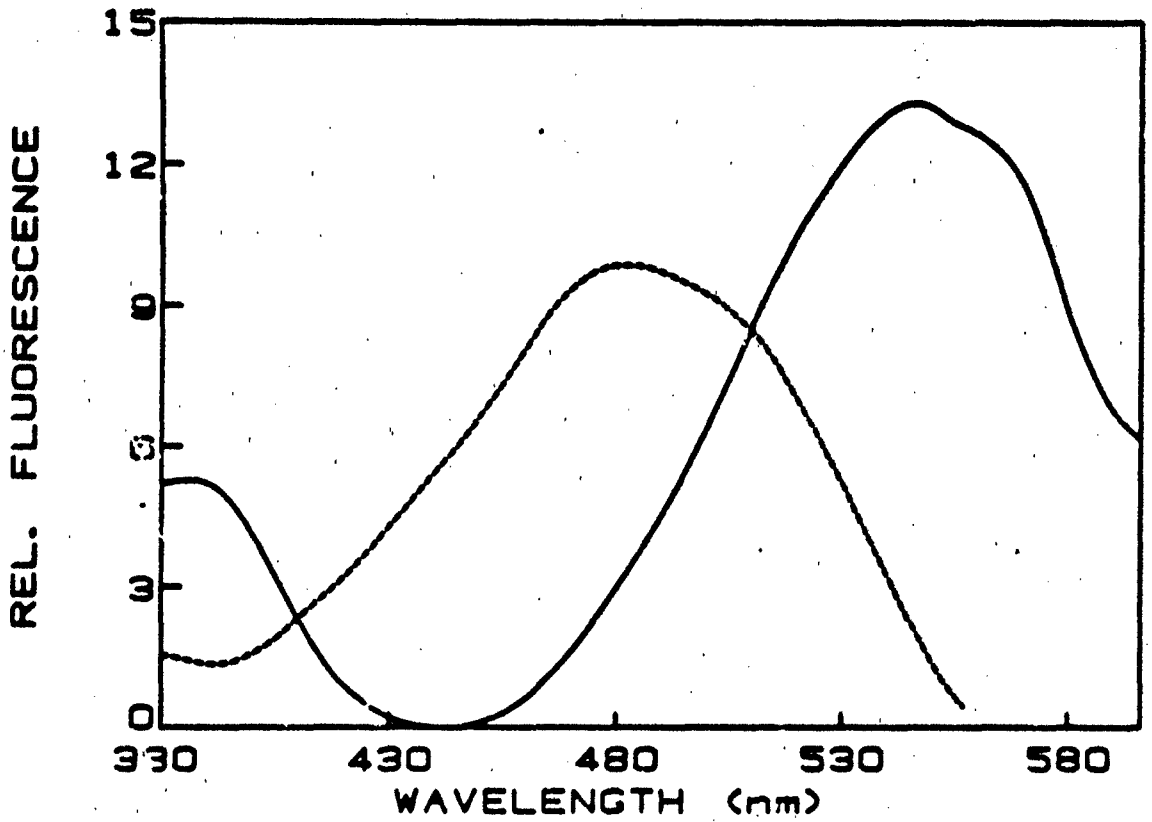

Fig. 11. Corrected-difference excitation spectra of decidium bound to the membrane-associated AChR. (- - -), Difference in spectra between samples (AChR, 1 μM, in α-toxin sites; decidium, 1 μM; PCP, 1 μM) in the absence and presence of carbachol (10 μM). (——), Difference in spectra between samples (AChR, 1 μM, in α-toxin sites; decidium, 1 μM; carbachol, 10 mM) in the absence and presence of PCP.

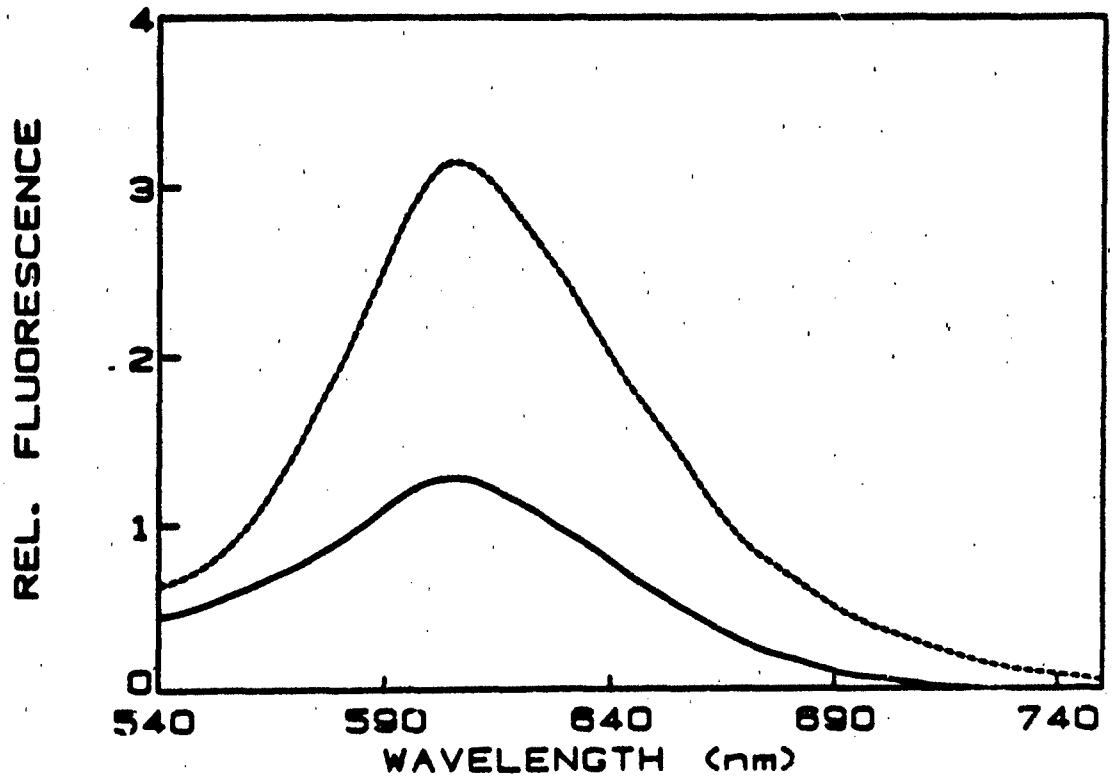

Fig. 12. Corrected-difference emission spectra of the decidium bound to the membrane-associated AChR. (- - -), Difference in spectra between samples (acetylcholine, 1 μM, in toxin sites; decidium, 1 μM; PCP, 1 μM) in the absence and presence of carbachol (1 μM). (——), Difference in spectra between samples (acetylcholine, 1 μM) in toxin sites; decidium, 1 μM; carbachol (10 mM) in the absence and presence of PCP.

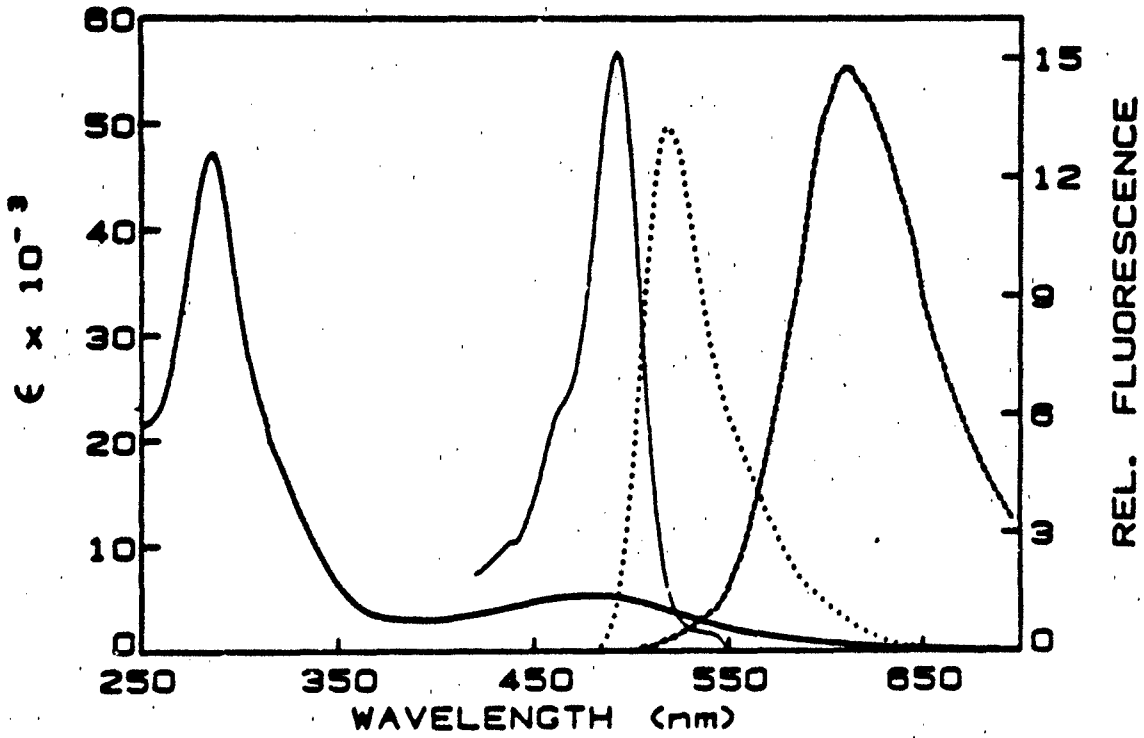

Fig. 13. Relationship between spectra of donor FITC-toxin and acceptor decidium energy transfer pair. The absorption spectra of donor (——) and acceptor (—·—·—) are presented as extinction coefficients ($M^{-1}.cm^{-1}$). The emission (corrected) of donor (····) and acceptor (uncorrected) (- - -) bound to the membrane-associated AChR are presented in arbitrary intensity units and are not shown in proportion to the relative quantum yield. All spectra were measured in 100 mM NaCl, 10 mM sodium phosphate at pH 7.4.

SECTION III

PROGRESS REPORT ON EFFORTS TO SITE-SPECIFICALLY LABEL COBRA α-TOXIN WITH FITC, EITC, AND TRITC

One of our major goals is to develop a "library" of site-specifically labeled α-toxins with which to examine the spatial relations between drug binding sites on the surface of the AChR by utilization of fluorescence energy transfer and quenching techniques. Specifically, we want to prepare at least three site-specifically labeled FITC conjugates and either three EITC or TRITC conjugates. We need only EITC or TRITC conjugates, because they are both excellent FITC energy acceptors. What follows summarizes the progress that we have made on the preparation of FITC, EITC and TRITC conjugates.

FITC Conjugates. We have isolated and characterized an FITC-N^{ϵ}-lysine-23-α-toxin, using classical CM-52 ion exchange chromatography [43]. The FITC-lysine-23 conjugate was prepared by reacting stoichiometric amounts of FITC with α-toxin, conjugated FITC-toxins were isolated with gel filtration chromatography, and the various conjugates were partially resolved with CM-52 chromatography. The elution profile of a CM-52 column is shown in Fig. 14. The major monoconjugate elutes in Peak 4. Column isoelectric focusing of Peak 4 indicates two components with isoelectric points of 9.5 and 9.3 (Fig. 14, left inset). The yield of 9.5 component was high enough to allow determination of the site of labeling, i.e., lysine 23. The other apparent monoconjugates elute in peaks 5 and 6. Further purification of these peaks with column isoelectric focusing gave yields too low to allow site determination using the above procedures.

Alternative procedures have been and are being utilized to enhance the yields and purity of conjugates with the FITC attached to sites other than the lysine 23. One approach was to perform the conjugation reaction in 8 M guanidine HCl in order partially to denature and expose additional reactive sites on the surface of the α-toxin. This approach failed because of an overall decrease in reactivity of FITC in the presence of guanidine HCl. Another approach involved the use of BIO-REX 70 ion exchange chromatography, which has been shown to resolve biotinyl toxin derivatives [64]. Unfortunately, FITC is very hydrophobic compared to biotin and, consequently, FITC-toxin derivatives bind almost irreversibly to the hydrophobic matrix of the resin. Most recently, we have started to use citraconic anhydride to reversibly modify the highly reactive primary amino groups in the toxin so that the less reactive groups can be conjugated with FITC. The basic citraconic anhydride reaction is shown in Fig. 15. The citraconic anhydride reacts with primary amino groups, leaving a moiety with a free carboxylate. (The free carboxylate would be expected to decrease the isoelectric point of the peptide.) Following the citraconic anhydride reaction, FITC is allowed to react with the α-toxin, and the citraconic anhydride is removed with strong acid.

Fig. 16 shows that we can modify the toxin with citraconic anhydride. α-toxin was incubated with various concentrations of citraconic anhydride and the reaction products were resolved with Serva polyacrylamide isoelectric focusing plates. Native α-toxin focuses with any isoelectric point of about 10.1 with the Serva plates. Citraconic anhydride conjugation shifts the

isoelectric focusings to a variety of lower pH values, suggestive of the formation of multiple conjugates.

Fig. 17 shows the effect of increasing concentrations of FITC on the formation of FITC-toxin conjugates. As the molar fraction of FITC to α-toxin increased, so did the number of conjugates with lower isoelectric points. Presumably, as the positively charged toxin-amino groups are conjugated with the negatively charged FITC molecules, more derivatives are resolved with lower isoelectric points. Mono-FITC conjugates should focus with focusing points greater than 7. We resolved only one broad band with a focusing point of about 8.3. The elution profile of column isoelectric-focused (pH range 8-10) aliquot of the sample run in lane #2 (Fig. 17) is show in the right panel of Fig. 16. What appeared as a single broad band at pH 8.3 with the Serva plates (pH from 3 to 10) partially resolves into two bands with focusing points of about 9.3 and 9.0. While the 9.3 band probably represents a single monoconjugate, the 9.0 band includes at least three closely focused bands. The appearance of these bands prior to draining the isoelectric focusing column is shown in Fig. 19.

(The differences in isoelectric focusing values indicated by the Serva plates and column isoelectric focusing are repeatable and probably reflect the interactions of the two types of supports, polyacrylamide vs. sucrose, with the peptides.)

Because the band that focused at 9.3 did not focus at the same point (9.5) as FITC-lysine-23-toxin, prepared without citraconic anhydride modification, we initially thought that we had a partially isolated new monoconjugate. However, sequencing of the 9.3 band after column refocusing indicated that the FITC was attached to lysine 23. The CM-52 column appears to modify the FITC-lysine-23-α-toxin slightly to produce a shift in the focusing point, since we observed that column focusing noncitraconic-anhydride-modified α-toxin generated the major monoconjugated FITC-toxin with a focusing point of 9.3.

In summary, we have not yet isolated significant quantities of FITC derivatives conjugated at sites other than lysine 23. We have just started utilizing a new very high resolution isoelectric focusing technique developed by LKB called Immobiline. With this technique it should be possible to separate peptides with focusing points that differ by a few hundredths of a pH unit. I am optimistic that this technique will allow the isolation of at least two new FITC conjugates.

<u>EITC Conjugates</u>. Notwithstanding the high relative purity of commercial EITC in conjugating EITC to α-toxin, some labeling appears to have taken place, based both on the partial resolution of EITC-toxin reaction mixtures on Serva isoelectric focusing plates (Fig. 21) and on the elution profile from a CM-52 column. The major protein peak at about fraction 100 of the CM-52 column (Fig. 20), where one would anticipate at monoconjugate to elute, contained no components with focusing points greater than 6 (inset, Fig. 20). This suggests that the EITC (peak absorbance at 520 nm) nonspecifically partitioned into hydrophobic regions of the α-toxin. The column isoelectric focusing, which is usually the best means to dislodge noncovalently associated molecules from the α-toxin, separated all the EITC from the native α-toxin.

TRITC Conjugates. Compared to the FITC conjugation, relatively little work has been performed to label the α-toxin with TRITC, because we need to develop higher resolution techniques to separate the various monoconjugates. Column isoelectric focusing of the TRITC-toxin reaction mixture resolved six fluorescent bands prior to draining the column (Fig. 22). Analysis of the fractions collected indicated that the various bands merged into one ligand band (Fig. 23). As with the FITC-conjugation studies, we know that we can label more than one site on the surface of the α-toxin, but we need to develop a higher resolution technique to separate the various conjugates. The LKB Immobiline system is probably that technique.

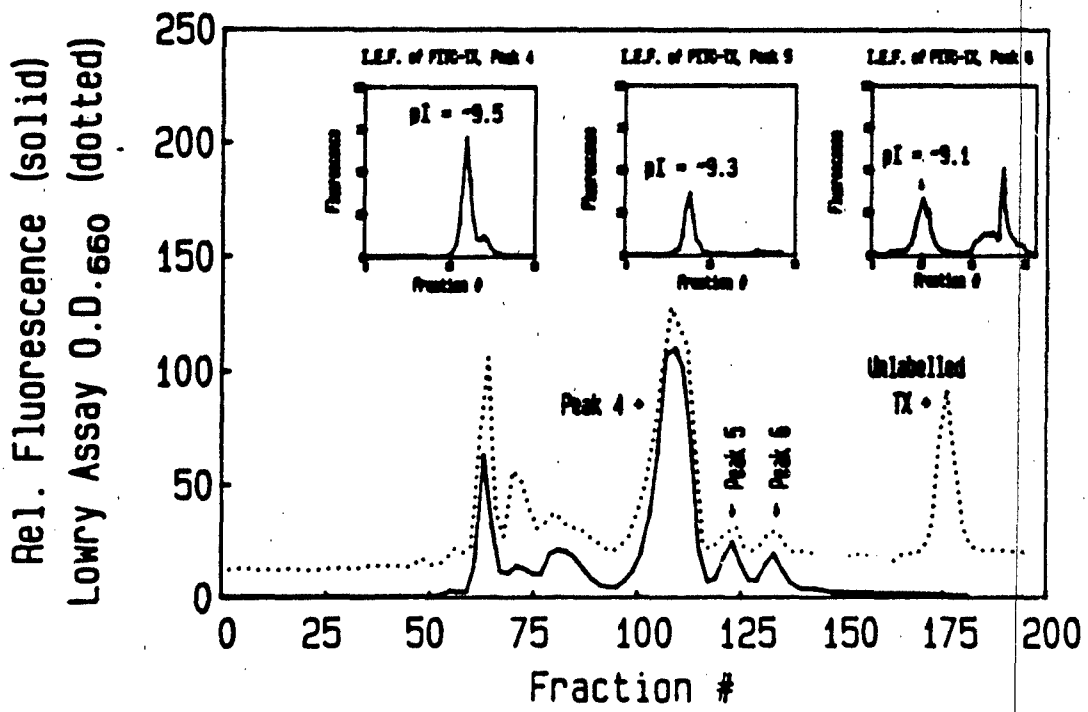

Fig. 14. CM-52 elution profile of FITC-labeled toxin: isoelectric focusing of Peaks 4, 5 and 6.

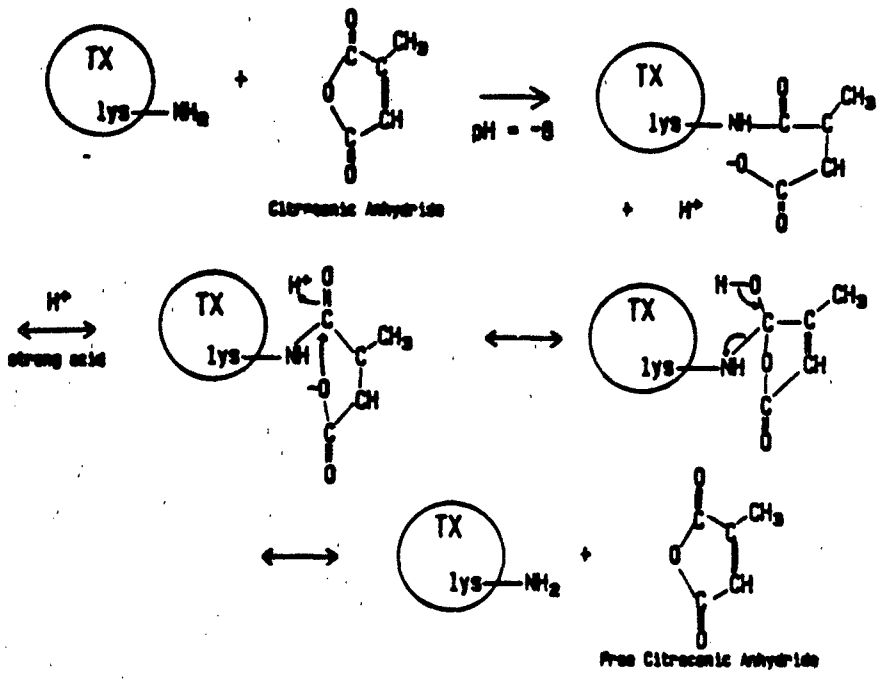

Fig. 15. Reaction scheme for citraconic anhydride modification.

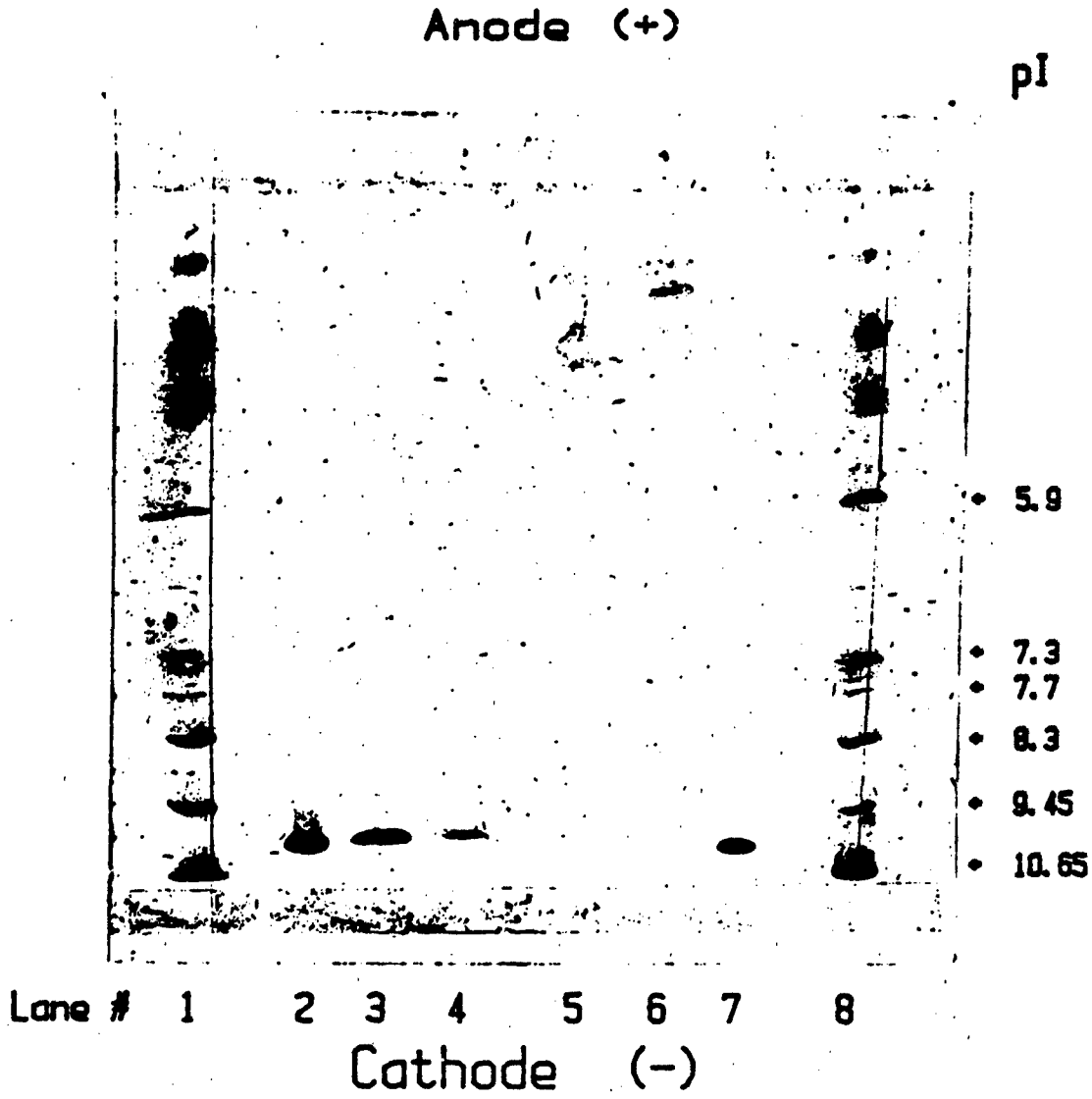

Fig. 16. Serva polyacrylamide isoelectric focusing of citraconic-anhydride-modified α-toxin. Lanes 1 and 8, protein standards. Lanes 2 and 7, native α-toxin. Lanes 3-6, increasing molar ratio of citraconic anhydride to α-toxin, 3, 10, 20 and 30.

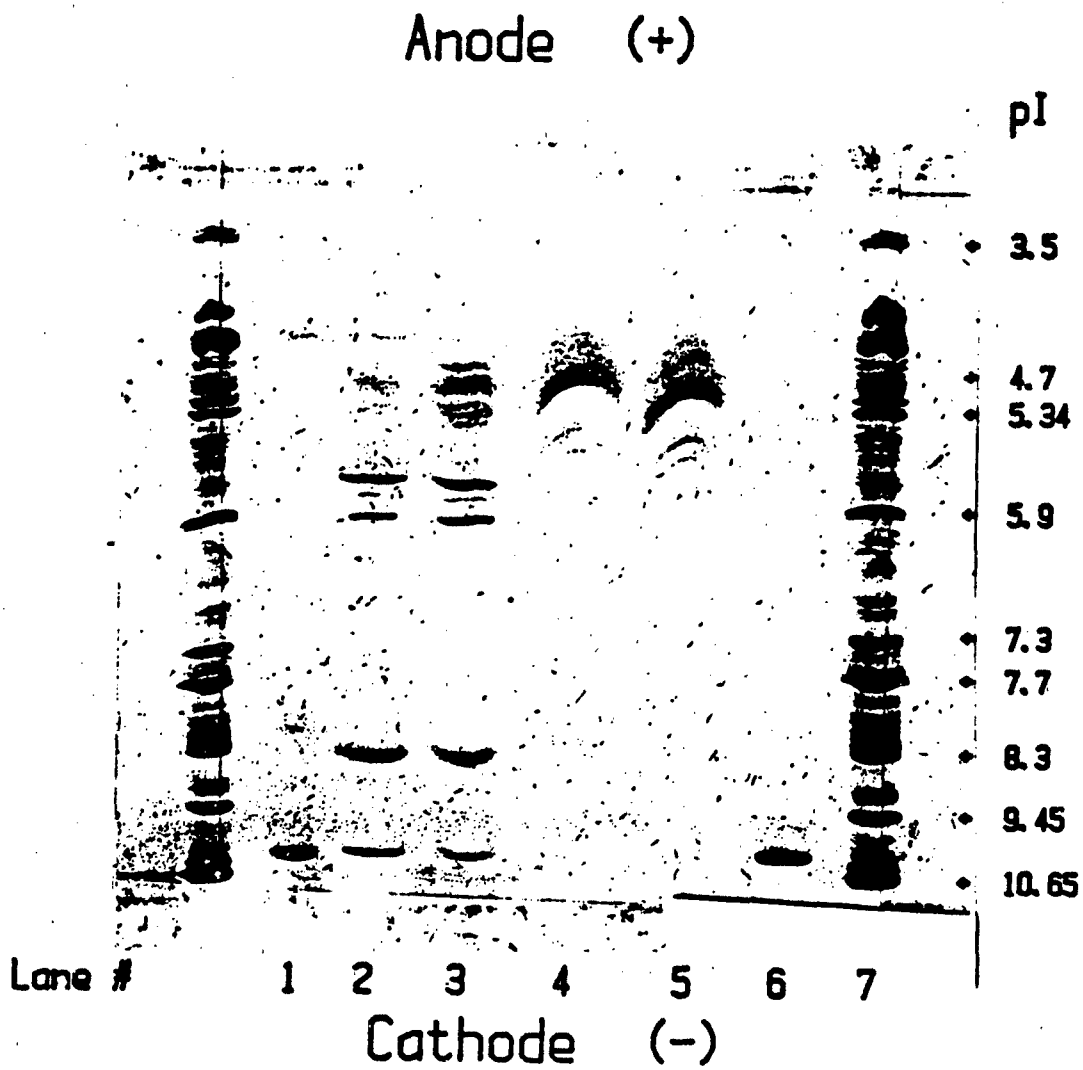

Fig. 17. Serva polyacrylamide isoelectric focusing of reaction mixtures of FITC and citraconic-anhydride-modified α-toxin. Lanes 0 and 7, protein standards. Lanes 1 and 6, native α-toxin. Lanes 2 to 5, increasing molar ratio of FITC to α-toxin, 1.5, 3, 6 and 9.

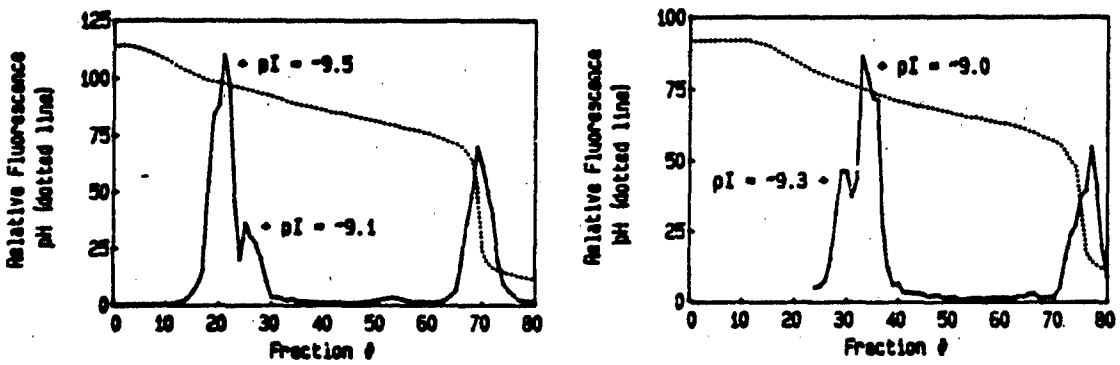

Fig. 18. IEF elution profile of the unmodified (left panel) and modified (right panel) FITC-toxin on an LKB 100 mL column.

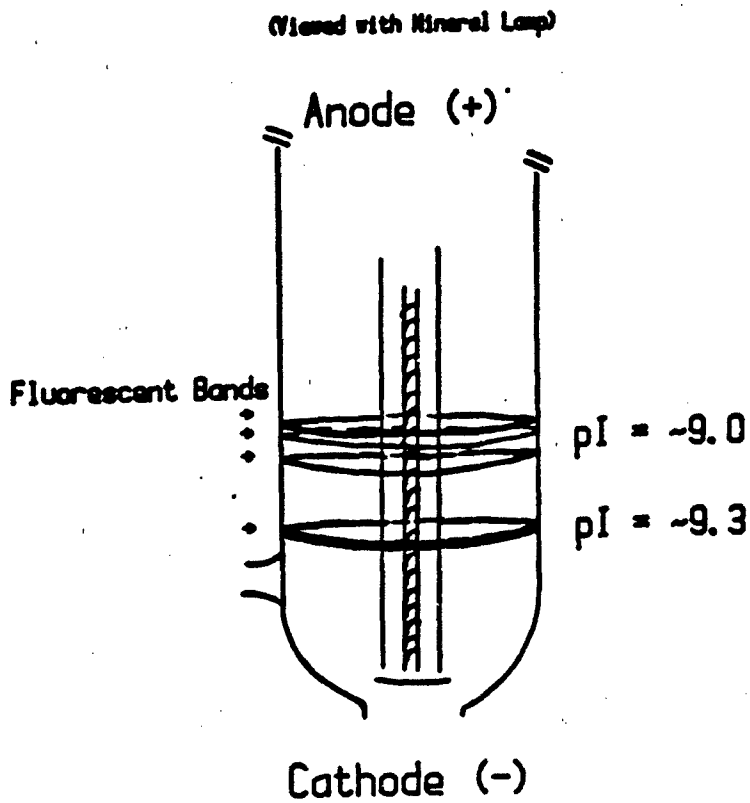

Fig. 19. Appearance of FITC-toxin reaction mixture on IEF column.

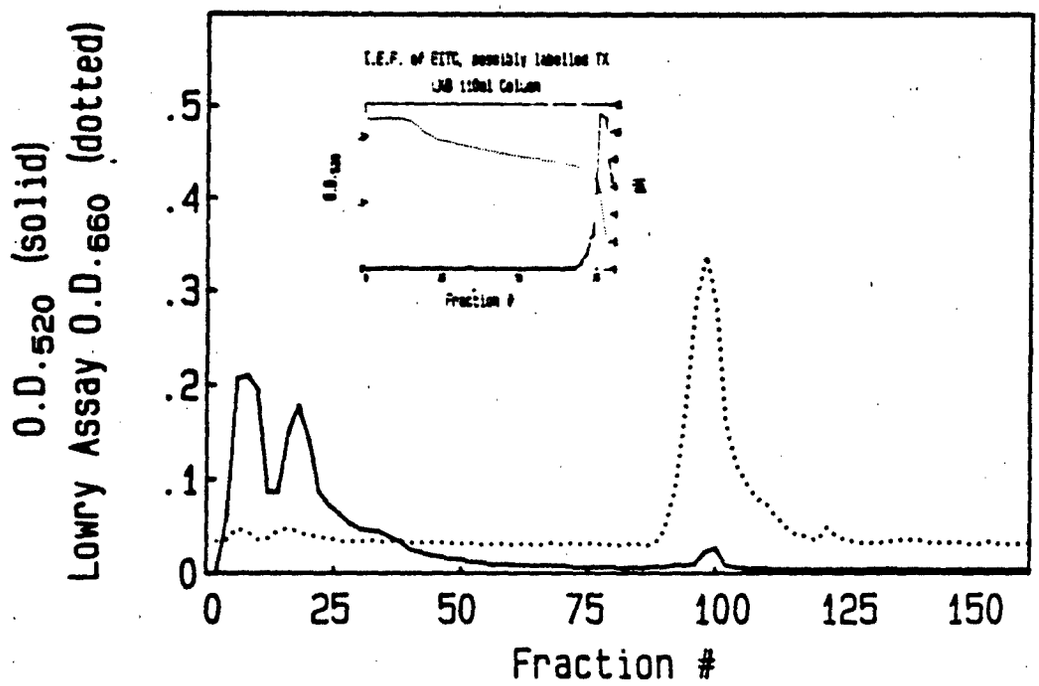

Fig. 20. Bio-Rex 70 elution profile of EITC-labeled toxin: isoelectric focusing of EITC-labeled toxin.

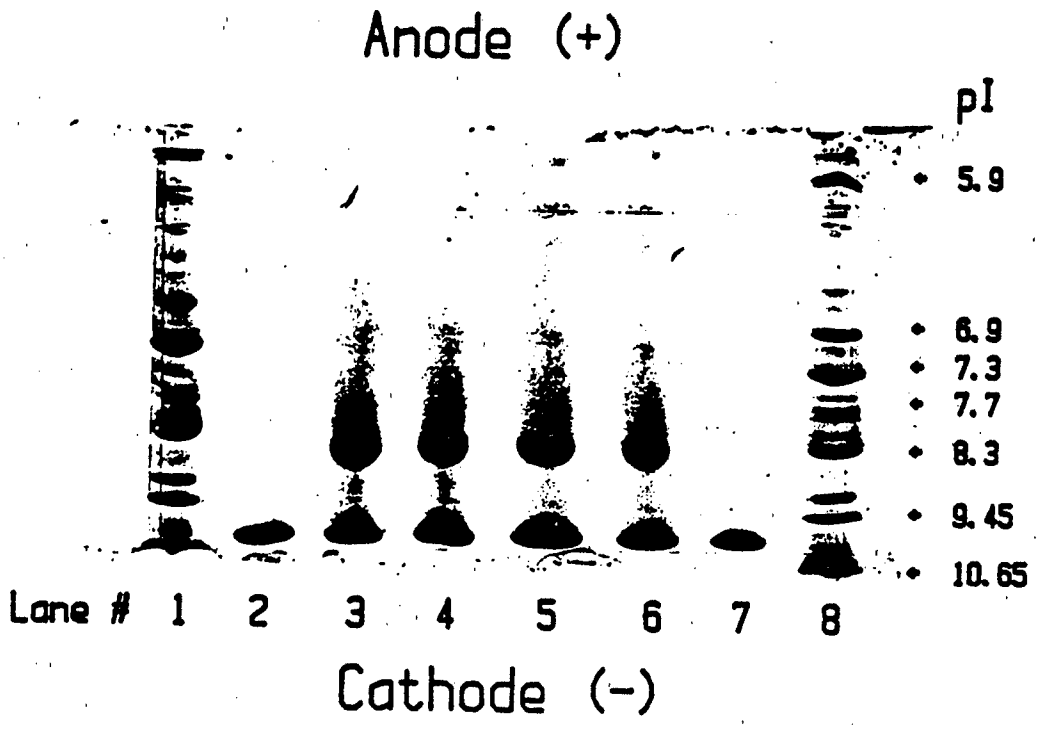

Fig. 21. Serva polyacrylamide isoelectric focusing resolution of the reaction mixture of EITC and α-toxin (2 to 1 mole ratio). Lanes 1 and 8, protein standards. Lanes 2 and 7, native α-toxin. Lanes 3 to 6, EITC α-toxin reaction mixture.

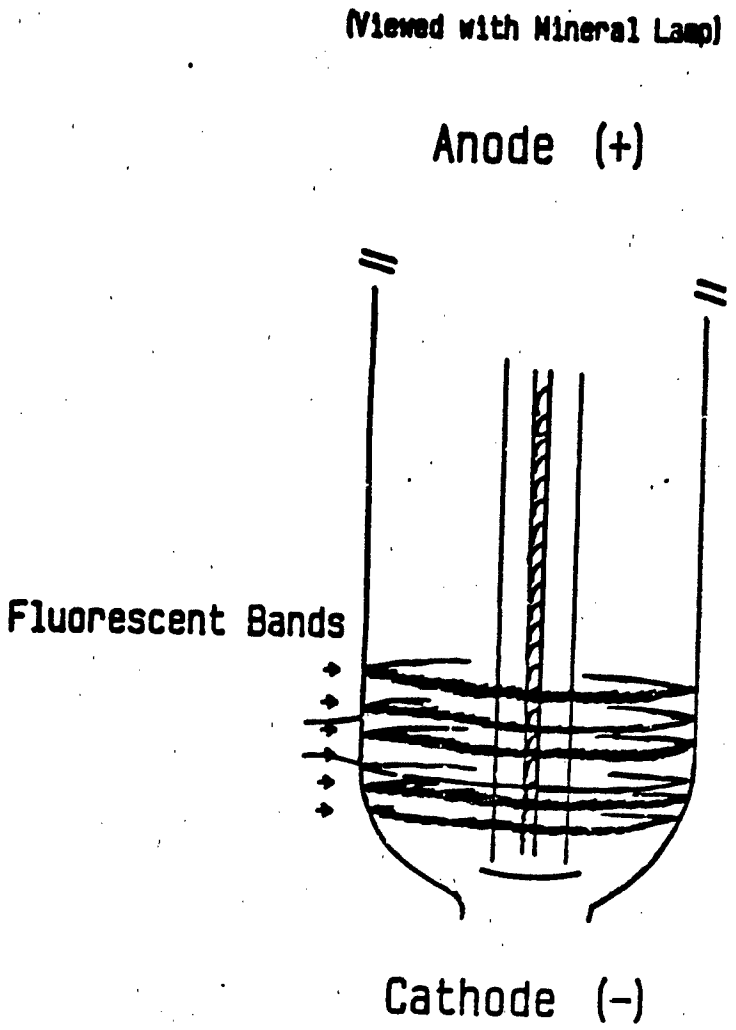

Fig. 22. Appearance of TRITC-toxin on column (viewed with mineral lamp).

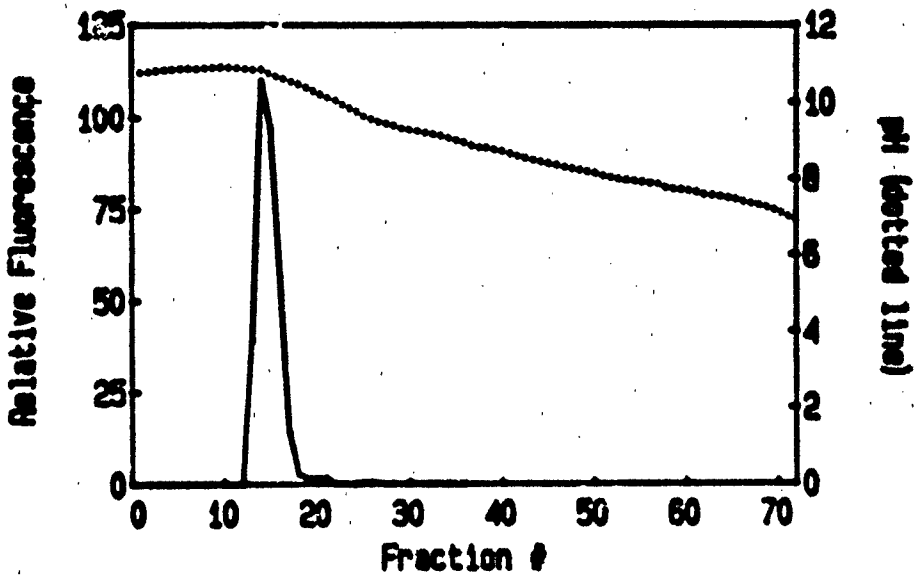

Fig. 23. Column IEF elution profile of TRITC toxin reaction mixture.

BIBLIOGRAPHY

1. Lester, H.A., J.P. Changeux and R.E. Sheridan. 1975. Conductance increases produced by both application of cholinergic agonists to Electrophorus electroplaques. J. Gen. Phys., 65:797-816.

2. Karlin, A. 1980. Molecular properties of nicotinic acetylcholine receptors. In: Cell Surface and Neuronal Function (Cotman, Poste, and Nicolson, eds.), Vol. 5, pp. 191-2560, Elsevier/North Holland, New York.

3. Taylor, P., R.D. Brown and D.A. Johnson. 1982. The linkage between ligand occupation and response of the nicotinic acetylcholine receptor. In: Current Topics in Membrane Receptors and Transport (A. Kleinzeller, ed.), Vol. 18, Ch. 15, pp. 407-443.

4. Lee, T., V. Witzemann, M. Schmierlik and M.A. Rafferty. 1977. Ligand interactions with cholinergic receptor enriched membranes from Torpedo: Influence of agonist exposure on receptor properties. Arch. Biochem. Biophys., 183:57-72.

5. Weiland, G., B. Georgia, V.T. Wee, C.F. Chignell and P. Taylor. 1976. Ligand interactions with cholinergic receptor-enriched membranes from Torpedo: Influence of agonist exposure on receptor properties. Mol. Pharmacol., 12:1091-1105.

6. Bonner, R., F.J. Barrantes and T.M. Jovin. 1976. Kinetics of agonist-induced intrinsic fluorescence changes in membrane-bound acetylcholine receptor. Nature (lond.), 263:429-431.

7. Barrantes, F.J. 1976. Intrinsic fluorescence of the membrane-bound acetylcholine receptor: Its quenching by Suberyldicholine. Biochem. Biophys. Res. Commun., 72:479-488.

8. Grunhagen, H.H. and J.P. Changeux. 1976. Studies on the electric action of acetylcholine with Torpedo marmorata electric organ: V. Qualitative correlation between pharmacological effects and equilibration processes of the cholinergic receptor protein as revealed by the structural probe quinacrine. J. Membr. Biol., 106:577-535.

9. Weill, C.L., M.G. McNamee and A. Karlin. 1974. Affinity-labeling of purified acetylcholine receptor from Torpedo californica. Biochem. Biophys. Res. Commun., 61:997-1003.

10. Raftery, M.A., R.L. Vandlen, K.L. Reed and T. Lee. 1975. Characterization of Torpedo californica acetylcholine receptor: Its subunit composition and ligand-binding properties. Sym. Quant. Biol., 40:193-202.

11. Damle, V., M. McLaughlin and A. Karlin. 1978. Bromoacetylcholine as an affinity label of the acetylcholine receptor from Torpedo californica. Biochem. Biophys. Res. Commun., 84:845-851.

12. Reynolds, J. and A. Karlin. 1978. Molecular weight in detergent solution of acetylcholine receptor. Biochemistry, 17:2035-2038.

13. Schiebler, W., L. Lauffer and F. Hucho. Acetylcholine receptor enriched membranes: Acetylcholine binding and excitability after reduction in vitro. FEBS Lett., 81:39-42.

14. Noda, M., H. Takahashi, T. Taube, M. Toyosata, Y. Furutani, T. Hirsoe, M. Asai, S. Inayama, T. Miyata and S. Numa. 1982. Cloning and sequence analysis of calf cDNA and human genomic DNA encoding α-subunit precursor of Torpedo californica acetylcholine receptor deduced from cDNA sequence. Nature (Lond.), 299:793-797.

15. Noda, M., H. Takahashi, T. Taube, M. Toyosato, S. Kikyotani, T. Hirose, M. Asai, H. Takashim, S. Inayama, T. Miyata and S. Numa. 1983. Primary structure of α-subunit precursor of Torpedo californica acetylcholine receptor deduced from a cDNA sequence. Nature (Lond.), 301:251-255.

16. Claudio, t., M. Ballivet, J. Patrick and S. Heinemann. 1983. Nucleotide and deduced amino acid sequence of Torpedo californica acetylcholine receptor α-subunit. Nature (Lond.), 80:1111-1115.

17. Nathanson, N.M. and S.W. Hall. 1979. Subunit structure and peptide mapping of junctional and extrajunctional acetylcholine receptors from rat muscle. Biochemistry, 18:3392-3401.

18. Froehner, S.C. and S. Rafto. 1979. Comparison of the subunits of Torpedo californica acetylcholine receptor by peptide mapping. Biochemistry, 18:301-307.

19. Lindstrom, J., B. Einarson and J. Merlie. 1978. Immunization of rats with polypeptide chains from Torpedo acetylcholine receptor causes an autoimmune response to receptors in rat muscle. Proc. Natl. Acad. Sci. USA, 75:769-773.

20. Neubig, R.R., E.K. Krodel, N.D. Boyd and J.B. Cohen. 1979. Acetylcholine and local anesthetic binding to Torpedo nicotinic post-synaptic membranes after removal of non-receptor peptides. Proc. Natl. Acad. Sci. USA, 76:690-694.

21. Ross, M.J., M.W. Klymkowsky, D.A. Agard and R.M. Stround. 1977. Structural studies of a membrane-bound acetylcholine receptor from Torpedo californica. J. Membr. Biol., 116:635-659.

22. Raftery, M.A., J. Schmidt and D.G. Clark. 1972. Specificity of α-bungarotoxin binding to Torpedo californica electroplate. Arch. Biochem. Biophys., 152:882-886.

23. Changeux, J.-P., E.L. Bendetlig, J.-P. Bourgeois, A. Brusson, J. Cartaud, P. Devaux, H. grunhagen, M. Moreau, J.-L. Popot, A. Sobel and M. Weber. 1979. Some structural properties of the cholinergic receptor protein in its membrane environment relevant to its function as a pharmacological receptor. Symp. Quant. Biol., 40:211-230.

24. Eldefrawi, M.E., A.T. Eldefrawi, N.A. Mangour, J.W. Daly, B. Witkop and E.X. Albuquerque. Acetylcholine receptor and ionic channel of Torpedo electroplax: Binding of perhydrohistrion.cotoxin to membrane and solubilized preparations. Biochemistry, 17:5475-5484.

25. Krodel, E.K., R.A. Beckmann and J.B. Cohen. 1979. Identification of a local anesthetic binding site in nicotinic post-synaptic membranes isolated from Torpedo marmorata electric tissue. Mol. Pharmacol., 15:294-312.

26. Neubig, R.R. and J.B. Cohen. 1979. Equilibrium binding of [^{3}H] tubocurarine and [^{3}H]acetylcholine by Torpedo postysynaptic membranes: Stoichiometry and ligand interactions. Biochemistry, 18:5464-5474.

27. Sine, S. and P. Taylor. 1982. Local anesthetics and histrionicotoxin are allosteric inhibitors of the acetylcholine receptor. J. Biol. Chem., 257:8106-8114.

28. Sine, S. and P. Taylor. 1981. Relationship between reversible antagonist occupancy and the functional capacity of the acetylcholine receptor. J. Biol. Chem., 256:6692-6698.

29. Wennogle, L.P. and J.P. Changeux. 1980. Transmembrane orientation of proteins present in acetylcholine receptor rich membranes from Torpedo mormorata studied by selective proteolysis. Eur. J. Pharmacol., 106:381-393.

30. Strader, C.D. and M.A. Raftery. 1980. Topographic studies of Torpedo acetylcholine receptor subunits as a transmembrane complex. Proc. Natl. Acad. Sci. USA, 77:5807-5811.

31. Tarrab-Hadzai, R., B. Geiger, S. Fuchs and A. Amsterdam. 1978. Localization of acetylcholine receptor in excitable membrane from the electric organ of Torpedo. Evidence for exposure of receptor antigenic sites on both sides of the membrane. Proc. Natl. Acad. Sci. USA, 75:2497-2501.

32. Strader, C.B.D., J.P. Ruvel and M.A. Raftery. 1979. Demonstration of the transmembrane nature of the acetylcholine receptor by labeling with anti-receptor antibodies. J. Cell Biol., 83:499-510.

33. Forehmer, S.C. 1981. Identification of exposed and buried determinants of the acetylcholine receptor. Biochemistry, 20:4905-4915.

34. Hamilton, S.L., M. McLaughlin and A. Karlin. 1978. Crosslinking of the acetylcholine receptor. Fed. Proc., 37:528a.

35. Witzemann, V. and M.A. Raftery. 1978. Affinity directed crosslinking of acetylcholine receptor polypeptide components in post-synaptic membranes. Biochem. Biophys. Res. Commun., 85:623-731.

36. Zingsheim, H.P., F.J. Barrantes, J. Frantz, W. Hanicke and D.Ch. Neugebauer. 1982. Direct structural localization of two toxin-recognition sites on an ACh receptor protein. Nature, 299:81-84.

37. Sator, V., J.M. Gonzalez-Ros, P. Galuo-Fernandez and M. Martinez-Carrion. 1979. Pyrenesulfonyl azide: A marker of acetylcholine receptor subunits in contact with membrane hydrophobic environment. Biochemistry, 18:1200-1206.

38. Oswald, R. and J.-P. Changeux. 1981. Ultraviolet light-induced labeling by noncompetitive blockers of the acetylcholine receptor. Proc. Natl. Acad. Sci. USA, 78:3925-3929.

39. Forster, T. 1948. Intermolecular energy migration and fluorescence. Ann. Physik., 2:55-75.

40. Stryer, L. 1978. Fluorescence energy transfer as a spectroscopic ruler. Ann. Rev. Biochem., 47:819-846.

41. Berman, H.A., J. Yguerabide and P. Taylor. 1980. Fluorescence energy transfer on acetylcholinesterase: Spatial relationship between peripheral site and active center. Biochemistry, 19:2226-2235.

42. Pesce, A.J., C.-G. Rosen and T.L. Pasby. 1971. Fluorescence Spectroscopy, Marcel Dekker Inc., New York, pp. 177-178.

43. Johnson, D.A. and P. Taylor. 1982. Site-specific fluorescein-labeled cobra α-toxin. J. Biol. Chem., 257:5632-5636.

44. Burrage, T.G., T.L. Lentz, K. Moreno and G.H. Tignor. 1981. Binding of rabies virus to sites of high acetylcholine receptor density on cultured chick myotubes. J. Cell Biol., 91:86a.

45. Schurr, J.M. and K.S. Schmitz. 1976. Orientation constraints and rotational diffusion in bimolecular solution kinetics. A simplification. J. Phys. Chem., 80:1934-1936.

46. Shoup, D., G. Lipari and A. Szabo. 1981. Diffusion-controlled biomolecular reaction rates: The effect of rotational diffusion and orientation constraints. Biophys. J., 36:697-714.

47. Solc, K. and W.H. Stockmaker. 1971. Kinetics of diffusion-controlled reaction between chemically asymmetric molecules I. General theory. J. Chem. Phys., 54:2981-2988.

48. Solc, K. and W.H. Stockmaker. 1973. Kinetics of diffusion-controlled reaction between chemically asymmetric molecules. II. Approximate steady-state solution. Int. J. Chem. Kinetics, 5:733-752.

49. Abramowitz, M. and I.A. Stegun. 1965. Handbook of Mathematical Functions with Formulas, Graphs, and Mathematical Tables. Dover Publications, Inc., New York.

50. Cheung, A.T., D.A. Johnson and P. Taylor. 1983. Kinetics of interaction of N^{ϵ}-fluorescein isothiocyanate-lysine-23-cobra-α-toxin with the acetylcholine receptor. Biophys. J., 45:447-454.

51. Johnson, D.A. and J. Yguerabide. 1985. Solute accessibility to N^{ϵ}-fluorescein isothiocyanate-lysine-23-cobra α-toxin bound to the acetylcholine receptor: A consideration of the effect of rotational diffusion and orientation constraints on fluorescence quenching. Biophys. J., 46:949-955.

52. Karlsson, E., K. Arnberg and D. Eaken. 1971. Isolation of the principal neurotoxin of two Naja naja subspecies. Eur. J. Biochem., 21:1-16.

53. Weiland, G.B., B. Georgia, S. Lappi, C.F. Chignell and P. Taylor. 1977. Kinetics of agonist-mediated transitions in state of the cholinergic receptor. J. Biol. Chem., 252:7648-7656.

54. Reed, K., P. Vandlen, J. Bode, J. Duguid and M.A. Raftery. 1975. Characterization of acetylcholine receptor-rich and acetylcholinesterase-rich membrane particles from Torpedo californica electroplax. Arch. Biochem. Biophys., 167:138-144.

55. Schmidt, J. and M.A. Raftery. 1973. A simple assay for the study of solubilized acetylcholine receptors. Anal. Biochem., 52:349-355.

56. Yguerabide, J. 1972. Nanosecond fluorescence spectroscopy of macromolecules. Methods Enzymol., 26:498-578.

57. Rang, H.P. and Ritter. 1970. The relationship between desensitization and the metaphilic effect at cholinergic receptors. Mol. Pharmacol., 6:357-382.

58. Yguerabide, J. and E.E. Yguerabide. 1984. Nanosecond fluorescence spectroscopy in biological research. In: Optical Technic., J. Doyle, editor. Academic Press.

59. Brown, R.D. and P. Taylor. 1983. The influence of antibiotics on agonist occupation and functional states of the nicotinic acetylcholine receptor. Mol. Pharmacol., 23:8-16.

60. Tsetlin, V.I., E. Karlsson, Yu.N. Utkin, K.A. Pluzhnikov, A.S. Arseniev, A.M. Surin, V.V. Kondakov, V.F. Bystrov, V.T. Ivanov, Yu.A. Ovchinnikov. 1982. Interacting surfaces of neurotoxins and acetylcholine receptor. Toxicon., 20:83-93.

61. Heidmann, T., R.E. Oswald and J.-P. Changeux. 1983. Multiple sites of action for noncompetitive bio???? on acetylcholine receptor rich membrane fragments from Torpedo marmorata. Biochemistry, 22:3112-3127.

62. Herz, J.H., D.A. Johnson and P. Taylor. 1987. Interaction of noncompetitive inhibitors with the acetylcholine receptor. J. Biol. Chem., 262:7238-7247.

63. Domle, V.N. and A. Karlin. 1978. Affinity labeling of one of two α-hemotoxin binding sites in acetylcholine receptor from Torpedo californica. Biochemistry, 17:2039-2045.

64. Karlsson, E., D. Eaken and G. Ponterius. 1972. Modification of amino groups in naja naja neurotoxins and the preparation of radioactive derivatives. Biochim. Biophys. Acta, 257:235-248.

LIST OF ABBREVIATIONS

ACh	Acetylcholine
AChR	Nicotinic Acetylcholine Receptor
α-toxin	Cobra α-toxin (*siamensis* 3)
FITC	Fluorescein Isothiocyanate
EITC	Erythrosin Isothiocyanate
TRITC	Tetramethylrhodamine Isothiocyanate
IEF	Isoelectric Focusing
PCP	Phencyclidine
pI	Isoelectric focusing point
NBD	7-nitrobenzo-2-oxa-1,3-diazole

DISTRIBUTION LIST

1 copy	Commander US Army Medical Research and Development Command ATTN: SGRD-RMI-S Fort Detrick, Frederick, Maryland 21701-5012
5 copies	Commander US Army Medical Research and Development Command ATTN: SGRD-PLE Fort Detrick, Frederick, Maryland 21701-5012
12 copies	Defense Technical Information Center (DTIC) ATTN: DTIC-DOAC Cameron Station Alexandria, VA 22304-6145
1 copy	Dean School of Medicine Uniformed Services University of the Health Sciences 4301 Jones Bridge Road Bethesda, MD 20814-4799
1 copy	Commandant Academy of Health Sciences, US Army ATTN: AHS-CDM Fort Sam Houston, TX 78234-6100